REPORT DOCUMENTATION PAGE

Form Approved OMB No. 0704-0188

1. REPORT DATE *(DD-MM-YYYY)*	2. REPORT TYPE	3. DATES COVERED *(From – To)*
28-03-2006	Final Report	20 March 2003 - 25-May-06

4. TITLE AND SUBTITLE

A Unified View of Global Instability of Compressible Flow over Open Cavities

5a. CONTRACT NUMBER
FA8655-03-1-3059

5b. GRANT NUMBER

5c. PROGRAM ELEMENT NUMBER

6. AUTHOR(S)

Dr. Vassilios Theofilis

5d. PROJECT NUMBER

5d. TASK NUMBER

5e. WORK UNIT NUMBER

7. PERFORMING ORGANIZATION NAME(S) AND ADDRESS(ES)

Nu-modeling, Inc.
C/. Mariano Barbacid No 1 Puerta 9
Boadilla del Monte (Madrid) E-28660
Spain

8. PERFORMING ORGANIZATION REPORT NUMBER

N/A

9. SPONSORING/MONITORING AGENCY NAME(S) AND ADDRESS(ES)

EOARD
PSC 821 BOX 14
FPO 09421-0014

10. SPONSOR/MONITOR'S ACRONYM(S)

11. SPONSOR/MONITOR'S REPORT NUMBER(S)
Grant 02-3059

12. DISTRIBUTION/AVAILABILITY STATEMENT

Approved for public release; distribution is unlimited.

13. SUPPLEMENTARY NOTES

14. ABSTRACT

This report results from a contract tasking Nu-modeling, Inc. as follows: The contractor will investigate the global linear instability of three-dimensional flow over an open cavity to develop a unified framework for understanding and controlling cavity-driven instabilities. Specifically the contractor will: (1) Perform global instability analyses of the flow field in two-dimensional open cavities; (2) Investigate linear and nonlinear interaction of the modes using simplified models and compare with DNS results, and assess the limits of usefulness of existing empirical prediction models. (3) Perform two-dimensional DNS and global instability analysis of full-bay open-cavity models. Compare results with DNS and/or experiment, and propose adjustments of the empirical models. (4) Perform three-dimensional DNS in empty open cavities and classify global instabilities as functions of flow and geometric parameters. (5) Propose theoretically founded flow-control strategies for realistic geometries and flow conditions.

15. SUBJECT TERMS
EOARD, Flow Stability and Transition, Flow Instability

16. SECURITY CLASSIFICATION OF:			17. LIMITATION OF ABSTRACT	18, NUMBER OF PAGES	19a. NAME OF RESPONSIBLE PERSON
a. REPORT	b. ABSTRACT	c. THIS PAGE			SURYA SURAMPUDI
UNCLAS	UNCLAS	UNCLAS	UL	55	19b. TELEPHONE NUMBER *(Include area code)* +44 (0)20 7514 4299

FINAL REPORT

A Unified View of Global Instability of Compressible Flows over Open Cavities

Principal Investigator: Vassilis Theofilis, Ph. D.
Numerical Modelling, S.L. Mariano Barbacid No 1, Door 9,
E-28660 Boadilla del Monte (Madrid), Spain
Voice +34 627 915 423, Fax +34 91 336 3295
E-mail, vassilis@aero.upm.es

This document is the final report on research activities sponsored by the Air Force Office of Scientific Research, Air Force Material Command, USAF, under Grant number FA8655-03-1-3059, (European Office of Aerospace Research and Development Grant number 023059) entitled "A Unified View of Global Instability of Compressible Flow over Open Cavities". The Grant was managed by Dr. John Schmisseur of AFOSR, Mr Wayne Donaldson and Dr. Surya Surampudi of EOARD. A coordinated activity on the same topic was supported in parallel at the California Institute of Technology by Grant number F49620-02-1-0362; the results of the latter effort will be reported separately. The present report covers the 36-month period from March 21, 2003, the inception of the grant, to its end on March 20, 2006. This collaborative research was supported in order to combine, for the first time, BiGlobal linear stability theory and Direct Numerical Simulation and employ these tools to advance the understanding, classification and ultimate control of linear instabilities of compressible (subsonic) flows over open cavities. The topics investigated in the present research program are listed in Section IV of the Table of Contents below. Of these, the first 5 were contemplated in and followed the schedule of the original proposal; topics under section 6 have been realized as "targets of opportunity" that emerged, on the one hand by the need to complement, diversify and expand the activities in the collaborative research as stated in the proposal, and on the other hand from the maturing of the technologies necessary to perform the related state-of-the-art research. I certify that there were no subject inventions to declare during the performance of this Grant. The U.S. Government is authorized to reproduce and distribute reprints for Government purpose notwithstanding any copyright notation thereon. The views and conclusions contained herein are those of the author and should not be interpreted as necessarily representing the official policies or endorsements, either expressed or implied, of the Air Force Office of Scientific Research or the U.S. Government.

CONTENTS

I. EXECUTIVE SUMMARY

In the framework of the present Grant the scope of past investigations on instability of cavity flows has been broadened and unified under the point of view of (nonparallel) BiGlobal linear instability theory. The understanding and classification of hydrodynamic (shear-layer- and in particular wake-mode) and aeroacoustic instabilities has been advanced by the first application of the author's residuals algorithm to compressible open cavity flows. It has been shown that all known classes of linear instabilities of open cavity flows, as well as previously unknown linear disturbances in a cavity, may be encountered as particular features of the same BiGlobal eigenvector at appropriate parameter ranges.

The role of three-dimensionality on BiGlobal cavity flow instability has been examined; by reference to a theoretically and experimentally well-documented model problem it has been shown that linearly unstable eigendisturbances of the two-dimensional steady basic flow persist when that basic state becomes three-dimensional. This provided motivation for the development of the first direct solution of the BiGlobal eigenvalue problem in compressible flow. Accurate and efficient numerical tools were subsequently developed in order to address three-dimensional instability of both the classic (empty) as well as full-bay models of cavity flows. New linear instability mechanisms have been discovered and independently confirmed by a linearized Direct Numerical Simulation approach.

Probably the most directly relevant to Air Force applications aspect of the present research has been the first-ever linear instability analyses of full-bay cavity models. The key result obtained was the (not altogether unexpected) demonstration that the cavity geometry exerts a crucial influence on the principal instability characteristics of cavity eigendisturbances, namely their frequency, amplification rate and spatial structure of the modes' amplitude functions.

In this manner, at the conclusion of the Grant, we find ourselves a good deal closer to the stated ultimate objective of our research, namely the proposition of theoretically-founded flow-control strategies for realistic geometries and flow conditions relevant to Air Force applications. The present work has been the first to provide essential building blocks of such a strategy, which permit relaxing past restrictive assumptions on the form of the basic cavity flow, and could be integrated in flow-control strategies aiming at addressing real Air Force needs.

List of Tables

List of Figures

II. BACKGROUND AND MOTIVATION

Our concern in the framework of this Grant has been with hydrodynamic and aeroacoustic instabilities in compressible open cavity flow. Most theoretical work on this problem to-date has focused on a distinct feature of this flow, namely flow/acoustic resonance (Powell 1961; Rossiter 1964) through a feedback loop involving (i) excitation of the unstable shear layer emanating from the upstream corner of the cavity through a Kelvin-Helmholtz (KH) instability, (ii) generation of an unsteady irrotational field by interaction of the shear layer with a solid boundary, typically the downstream corner of the cavity and (iii) the upstream influence of the irrotational field which provides for the further excitation of the instabilities in the shear layer, especially near the upstream edge. For incompressible flow, the upstream influence is instantaneous, while for compressible flow there is an acoustic delay. Resonance occurs when the phase change of a disturbance, at a given frequency, leads to constructive reinforcement and, ultimately, saturation. Because of the coupling with flow instability, cavity resonant frequencies and amplitudes may depend on the flow speed, U, the boundary layer (momentum) thickness, θ, just upstream of the cavity, ambient density, ϱ_∞, viscosity, μ_∞, and sound speed, a_∞. For a two-dimensional rectangular cavity with length, L, and depth, D, there are thus four dimensionless parameters governing the flow L/D, L/θ, $Re_\theta = \varrho_\infty U\theta/\mu_\infty$, $Ma = U/ a_\infty$ as well as additional parameters and profiles that would specify the state of the boundary layer upstream of the cavity if it were turbulent. The instability mechanism proposed by Rossiter (i.e. a convectively unstable nearly-parallel, two-dimensional shear layer that is forced by the large acoustic field produced near the downstream interaction) is but one of several modes of instability that have been observed in flows over cavities.

Factors that determine what instability mechanism will be observed include all the relevant parameters discussed above. Even for shallow cavities (L/D > 1), Gharib and Roshko (1987) observed in their incompressible experiments on an axisymmetric cavity that, as the length of the cavity (relative to the upstream boundary layer thickness) was increased, there was a substantial change in the behavior of the cavity oscillations, denoted as "wake mode" by these authors. Under these conditions, the flow was characterized by a large scale (dimensions of the cavity depth) shedding from the cavity leading edge. In two-dimensional Direct Numerical Simulation (DNS), Rowley, Colonius and Basu (2002) have observed a very similar transition. In both experiment and computation, the boundary layer upstream of the cavity was laminar. The wake mode transition has also been observed in two-dimensional Reynolds averaged Navier-Stokes calculations at higher Reynolds numbers (Fuglsang and Cain 1992; Cain, Rubio, Bortz, Banks and Smith 2000; Shieh and Morris 2001). Rowley *et al.* (2002) have performed an extensive mapping of the transition to wake mode for two-dimensional flows in parameter space. A key discovery was that the frequency of oscillation in wake mode was found to be nearly constant with Mach number (from 0.4 to 0.8) and it would appear that the instability is in this regime is purely hydrodynamic in nature.

Recently Alvarez, Kerschen and Tumin (2004) have made progress in developing improved linear models of the scattering/receptivity, and acoustic propagation aspects of the Rossiter modes and are able to eliminate many of the empirical parameters in the original Rossiter model. However, when significant interactions between the shear layer and the flow within the cavity exist, the flow may be found in a state completely different from that of cavity resonance that can be described with the aid of the Rossiter model (or any of its improved versions), namely the wake mode of Gharib and Roshko (1987). The wake mode appears to be a global instability more akin to vortex shedding from bluff bodies; unlike the Rossiter mode the frequency of oscillation is independent of Mach number, indicating that acoustic feedback does not play a role in the instability. However, wake mode is not commonly observed in shallow cavity flows at moderate subsonic to supersonic Mach number. Further, it is clear that three dimensionality plays a key role. Work by Shieh and Morris (2000; 2001) has shown that two dimensional cavities that are oscillating in wake mode

return to the Rossiter mode when the incoming boundary layer has three dimensional disturbances; it is now generally accepted that the development of three-dimensionality in the resonant oscillations plays a role in suppressing the wake mode instability (Gloerfelt, Bogey, Bailly, and Juve 2002). On the other hand, it is remarkable, indeed, that the wake-mode oscillation seen in the two-dimensional simulations, is very similar to that which exists for deeper cavities that exhibit higher levels of acoustic forcing, such as the oscillations seen in gas flows in pipes with closed side branches (Kriesels, Peters, Hirshberg, Wijnands, Iafrati, Riccardi, Piva, and Bruggeman 1995). These are high-Reynolds number three-dimensional turbulent flows developing in a three-dimensional geometry. While such modes have apparently not been observed in shallow cavities at high Reynolds numbers, it is at present unclear under what flow conditions the transition should occur. Between the two extremes (Rossiter and wake mode) there is a large number of experimental observations that involve significant interactions between the shear layer dynamics and the flow within the cavity (e.g. Gloerfelt *et al.* 2002; Forestier, Jacquin and Geffroy 2003).

However, there is very little theory available with which to understand all instability modes of the cavity, their interaction and the potential impact of such interaction on quantities of interest such as frequency and amplitude of oscillations, interactions of multiple tones, loads on internal cavity surfaces, e.t.c. The combined efforts in the framework of the present and the associated Caltech Grants have aimed at filling this gap by calculating and understanding the instabilities and resonance of open cavities over the entire parameter space, including those regimes where significant shear layer and cavity interactions occur. A key element differentiating the current from previous theoretical efforts is the relaxation of the invariably used, in past stability analyses, parallel flow assumption. In the framework of the present effort, the eigenspectrum of the entire cavity steady flowfield has to be computed. This flowfield is inhomogeneous in at least two (streamwise and depth) spatial directions, making the open cavity an ideal candidate for the application of the BiGlobal linear theory concept, as discussed by Theofilis (2003).

Encouraging results in related flows have recently appeared in the literature. Work by Barkley, Gomes and Henderson (2002) on the global linear instability of incompressible flow in the backward-facing step geometry, which can be related with that of a wide open cavity at appropriate parameter ranges, has discovered the existence of amplified large-scale small-amplitude spanwise-periodic vortical structures, which are distinct from the small-scale KH-type of instability of the shear layer emanating from the lip of the step. This global instability is attributed to self-excitation and amplification of an eigenmode of the closed recirculation bubble formed between the lip and the downstream floor of the backward-facing step. An analogous mechanism has been proposed for the forward-facing step by Stüer, Gyr and Kinzelbach (2000). On the other hand, two different models of closed recirculation bubbles were independently shown by Hammond and Redekopp (1998) and Theofilis, Hein and Dallmann (2000) to support global linear instability, qualitatively analogous to that of flow in the backward-facing step. In particular, the latter work was the first to demonstrate the potential of a closed recirculation zone (a laminar separation "bubble") to become self-excited on account of a global instability, besides strongly amplifying incoming KH-type of disturbances. Recent work on this topic by Simens, González, Theofilis and Gómez-Blanco (2005) has established the capacity of BiGlobal linear theory to describe both classic (KH) and BiGlobal eigenmodes within a unified framework. In cavity flows, another interesting observation has been made in the experimental and numerical work of Jackson, Hillier and Soltani (2001) in two-dimensional hypersonic closed cavity flow, where Taylor-Görtler-like vortices forming in the floor of the cavity appear to be responsible for unsteadiness and three-dimensionality in the flow at low aspect ratios. As the aspect ratio increases the structure spreads and covers the entire cavity, while KH instability of the shear-layer only influences the laminar-turbulent transition process at very large cavity aspect ratios. The global linear instability mechanism of flow in the related lid-driven cavity model of a closed cavity flow is now well-understood from a theoretical point of view (Theofilis 2000; Theofilis, Duck and Owen 2004) and also has been verified experimentally (Benson and Aidun 1992).

Evidence on the existence of global modes in open cavities, prior to the first demonstration of their existence in the framework of the research reported herein, could be found in the literature. In several parameter regimes of an open cavity, modes of oscillation that exhibit features of both Rossiter mode and the wake mode have been observed. For a cavity with Ma = 0.8 and L/D = 0.42 (turbulent upstream boundary layer) Schlieren photographs by Forestier *et al.* (2003) show a flow structure that is clearly not describable in terms of the KH instability of a nearly parallel shear layer. Vortex roll-up near the leading edge resembles more closely that in the early stages of the wake mode cycle, as vortical structures are ejected into the free stream to a distance above the cavity which is a significant fraction of the cavity length. DNS of two dimensional cavities shows that in an intermediate parameter regime, the flow may exhibit wake mode intermittently, with relatively quiet periods dominated by shear layer instabilities in between.

The present theoretical effort rests on questioning a fundamental assumption of the vast majority of past cavity instability research. In analyzing the behavior of the shear layer, most investigators to-date have implicitly assumed that the shear layer behavior can be described in isolation from the geometric features, i.e. as if it were a free shear layer. Nonparallel effects, three-dimensionality, and the coupling of the flow inside the cavity are of course neglected in such analyses. An alternative analysis of the global instability modes, which requires spatial DNS as input, has been developed for the cavity by Theofilis (2000; 2003). The tool utilized to accomplish this task is the appropriate (in view of the inhomogeneous geometry) BiGlobal linear instability theory. In order to arrive at a unified stability theory of cavity flows, both the compressible residuals algorithm and direct solutions of the partial derivative EVP governing BiGlobal linear instability of nonparallel two-dimensional steady incompressible and compressible flows, have been utilized. As with any instability analysis, the first step has been calculation of the steady basic flow which, in the context of BiGlobal analysis, is obtained by two-dimensional DNS run to steady state (if one exists – more on this issue in Section III.2). In a second step, two- and three-dimensional instabilities may be calculated by numerical solution of the appropriate (partial-differential-equation-based) eigenvalue problem (EVP). Additionally, in view of the multi-parametric nature of the problem indicated above, efficient tools that minimize the computing work within the two-step approach discussed are needed. In the framework of the present Grant, we have extended the (EOARD-supported: F61775-99-W-E090 http://handle.dtic.mil/100.2/ADA379181) incompressible "residuals" algorithm to compressible flow; the compressible residuals algorithm then formed one of the pillars of the Caltech investigations.

A major thrust of the present Grant, not contemplated in the original proposal, but of sufficient interest in order to be pursued for over one-third of the duration of the Grant, has been the (worldwide first) investigation of the effect on instability characteristics (frequency and spatial distribution of the amplitude functions of the eigenmodes) of an (empty) open cavity, that objects placed inside the cavity may have. The technology developed herein has intended to, and to a large degree succeeded in merging the gap between the academic research capabilities existing prior to the present effort and the actual warfighter needs, in terms of direct prediction of eigenfrequencies (tones) of complex full-bay cavity configurations. At the conclusion of the Grant, we are in a position to perform BiGlobal instability analyses of relatively complex full-bay model configurations, under the sole assumption of a steady laminar (non-parallel) two-dimensional basic state. Analyses of time-periodic laminar or Reynolds-averaged turbulent basic flows are straightforward extensions of the present work, which would make use of the analysis tools developed herein. In what follows, the theoretical approaches used are briefly exposed in Section III, making reference to material published in the course of the present investigations for further details. In Section IV results obtained during the execution of the Grant are outlined, while emphasis is placed on the most novel development aspects of the present research, namely the spectral multi-domain algorithm which permits study of instability in complex cavity configurations. Our conclusions and projected outlook on future research is offered in Section V.

III. THEORETICAL APPROACHES

1. The compressible BiGlobal eigenvalue problem (EVP)

In the course of the Grant concluded, BiGlobal instability theory was applied for the first time to open cavity flows in both the incompressible and the compressible flow regimes. A review of this analysis methodology and its application to a wide spectrum of flows has been presented by Theofilis (2003). The analysis proceeds with the compressible equations of motion, from which the incompressible BiGlobal EVP may also be recovered. The equations, written for an arbitrary coordinate system, are

$$\begin{aligned}
\frac{\partial \rho}{\partial t} + \nabla \cdot (\rho \mathbf{u}) &= 0, \\
\frac{\partial (\rho \mathbf{u})}{\partial t} + \nabla \cdot (\rho \mathbf{u}\mathbf{u}) &= \frac{-1}{\gamma M^2} \nabla p \\
&\quad + \frac{1}{Re} \nabla \cdot \sigma, \\
\frac{\partial p}{\partial t} + \mathbf{u} \cdot \nabla p + \gamma p \nabla \cdot \mathbf{u} &= \frac{\gamma}{RePr} \nabla \cdot (\kappa \nabla T) \\
&\quad + \frac{\gamma(\gamma - 1) M^2}{Re} \Phi,
\end{aligned}$$

where shorthand notations, respectively, for the viscous stress tensor **σ,**

$$\sigma = \mu \left[(\nabla \mathbf{u} + \nabla \mathbf{u}^T) - \frac{2}{3} (\nabla \cdot \mathbf{u}) \, \mathbf{I} \right]$$

and the viscous dissipation function Φ,

$$\Phi = \frac{1}{2} (\nabla \mathbf{u} + \nabla \mathbf{u}^T) : \sigma$$

have been used.

Linear stability analysis in the BiGlobal framework involves the substitution of a decomposition of any of the independent flow variables, e.g. the three velocity components, temperature and pressure $\mathbf{q}(x,y,z,t) = (u, v, w, \theta, p)^T$ into the equations of motion. All quantities are considered to be composed of an O(1) steady two-dimensional basic state and small-amplitude O(ε) unsteady three-dimensional perturbations, according to the BiGlobal Ansatz shown in Table 1. In this table, single primes refer to time- or space-periodic quantities, and double primes refer to spatial coordinates with mild variation in comparison with that on the non-primed spatial coordinates. Note that the BiGlobal decomposition shown in Table 1 is applicable to both incompressible and compressible flows. In the compressible flow at hand, upon substitution into the general equations of motion of the BiGlobal instability Ansatz, use of a perfect-gas constitutive law and linearization, the compressible non-symmetric generalized linear BiGlobal EVP

$$\mathcal{L} \, \hat{\mathbf{q}} = \Omega \mathcal{R} \, \hat{\mathbf{q}},$$

for the determination of the complex eigenvalue $\Omega = \Omega r + i \, \Omega i$ results. In the temporal framework used, Ωr represents a frequency and Ωi the amplification/damping rate of the disturbance sought.

Table 1: Linear Stability Theory Decompositions.

Theory	Basic state		Eigenmode: Amplitude function		Eigenmode: Phase function		
TriGlobal	$\bar{\mathbf{q}}(x_1,x_2,x_3)$	+	$\hat{\mathbf{q}}(x_1,x_2,x_3)$	·	$\Theta_{3d}(t)$	;	$\Theta_{3d}=-\Omega t$
Parabolized Stability Equations - 3D	$\bar{\mathbf{q}}(x_1'',x_2,x_3)$	+	$\hat{\mathbf{q}}(x_1'',x_2,x_3)$	·	$\Theta_{2d}''(x_1'';t)$	;	$\Theta_{2d}''=\int_{x=x_0}^{x''}\alpha(\xi)\,d\xi-\Omega t$
BiGlobal Secondary Theory	$\bar{\mathbf{q}}(x_1,x_2,x_3';t')$	+	$\sum_{n=-\infty}^{\infty}\hat{\mathbf{q}}(x_1,x_2,x_3',t')$	·	$\Theta_{2d}'(t')$	;	$\Theta_{2d}'=\sigma t$
BiGlobal	$\bar{\mathbf{q}}(x_1,x_2)$	+	$\hat{\mathbf{q}}(x_1,x_2)$	·	$\Theta_{2d}(x_3;t)$	;	$\Theta_{2d}=\beta x_3-\Omega t$
Parabolized Stability Equations	$\bar{\mathbf{q}}(x_1'',x_2)$	+	$\hat{\mathbf{q}}(x_1'',x_2)$	·	$\Theta_{1d}''(x_1'',x_3;t)$	;	$\Theta_{1d}''=\int_{x=x_0}^{x''}\alpha(\xi)\,d\xi+\beta x_3-\Omega t$
Herbert Secondary Theory	$\bar{\mathbf{q}}(x_1',x_2;t')$	+	$\sum_{n=-\infty}^{\infty}\hat{\mathbf{q}}(x_1',x_2,t')$	·	$\Theta_{1d}'(x_3;t')$	;	$\Theta_{1d}'=\beta x_3-\sigma t$
Rayleigh / Orr-Sommerfeld	$\bar{\mathbf{q}}(x_2)$	+	$\hat{\mathbf{q}}(x_2)$	·	$\Theta_{1d}(x_1,x_3;t)$	;	$\Theta_{1d}=\alpha x_1+\beta x_3-\Omega t$

Explicitly, the EVP reads

$$\begin{pmatrix} \mathcal{L}_{x\hat{u}} & \mathcal{L}_{x\hat{v}} & \mathcal{L}_{x\hat{w}} & \mathcal{L}_{x\hat{\theta}} & \mathcal{IL}_{x\hat{p}} \\ \mathcal{L}_{y\hat{u}} & \mathcal{L}_{y\hat{v}} & \mathcal{L}_{y\hat{w}} & \mathcal{L}_{y\hat{\theta}} & \mathcal{IL}_{y\hat{p}} \\ \mathcal{L}_{z\hat{u}} & \mathcal{L}_{z\hat{v}} & \mathcal{L}_{z\hat{w}} & \mathcal{L}_{z\hat{\theta}} & \mathcal{IL}_{z\hat{p}} \\ \mathcal{L}_{e\hat{u}} & \mathcal{L}_{e\hat{v}} & \mathcal{L}_{e\hat{w}} & \mathcal{L}_{e\hat{\theta}} & \mathcal{IL}_{e\hat{p}} \\ \mathcal{JL}_{c\hat{u}} & \mathcal{JL}_{c\hat{v}} & \mathcal{JL}_{c\hat{w}} & \mathcal{JL}_{c\hat{\theta}} & \mathcal{L}^G_{c\hat{p}} \end{pmatrix} \begin{pmatrix} \hat{u} \\ \hat{v} \\ \hat{w} \\ \hat{\theta} \\ \hat{p} \end{pmatrix} = \Omega \begin{pmatrix} \mathcal{R}_{x\hat{u}} & 0 & 0 & 0 & 0 \\ 0 & \mathcal{R}_{y\hat{v}} & 0 & 0 & 0 \\ 0 & 0 & \mathcal{R}_{z\hat{w}} & 0 & 0 \\ 0 & 0 & 0 & 0 & \mathcal{IR}_{e\hat{p}} \\ 0 & 0 & 0 & \mathcal{JR}_{c\hat{\theta}} & \mathcal{R}^G_{c\hat{p}} \end{pmatrix} \begin{pmatrix} \hat{u} \\ \hat{v} \\ \hat{w} \\ \hat{\theta} \\ \hat{p} \end{pmatrix}$$

where the unknown vector in this formulation comprises disturbance velocity components and disturbance temperature, respectively corresponding to solution of the momentum and energy equations, and disturbance pressure, corresponding to the equation of continuity. The lack of boundary conditions for the latter quantity requires the use of staggered grids and a natural choice ensuring high accuracy on the minimum number of nodes possible is spectral collocation (Macaraeg, Streett and Hussaini 1988). Spectral collocation based on two-dimensional mapped Chebyshev Gauss-Lobatto (CGL) and Chebyshev Gauss (CG) grids is used for spatial discretization of the EVP, as shown in Figure 1.

Figure 1: Upper: The Chebyshev Gauss-Lobatto (CGL) and the Chebyshev Gauss (CG) points, respectively denoted by full and open circles. Lower: the resulting discretization on a two-dimensional CGL and a staggered two-dimensional CG grid.

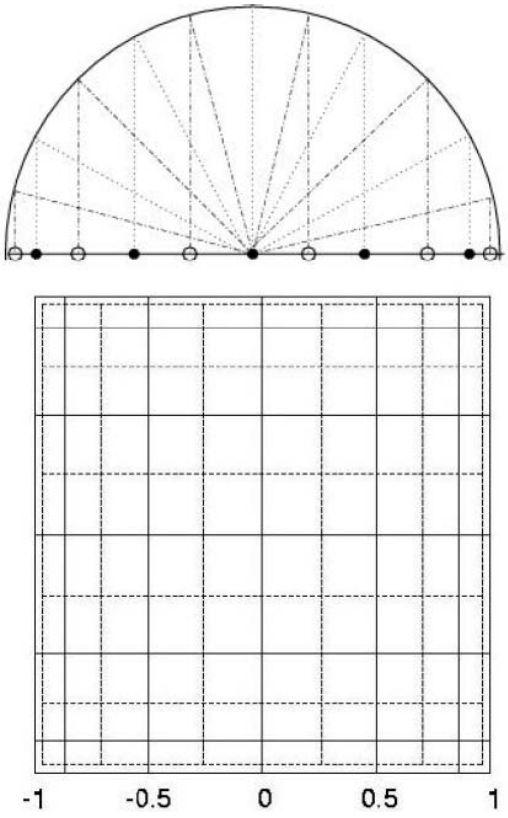

The CGL grid is used in order to collocate the disturbance momentum and energy equations, while the CG grid is used in order to collocate the disturbance continuity. The operators

$$\mathcal{I} = I_{GL}^{G},\ \mathcal{J} = I_{G}^{GL}$$

denote interpolation between the Chebyshev Gauss-Lobatto and Chebyshev Gauss grids and are used in order to transfer information between the two grids.

The linear operators are defined in the Appendix. Solution methods for the eigenvalue problem are discussed in detail by Theofilis (2003); a pictorial representation of the different paths followed is shown in Figure 2. Unless validation studies are performed, for which the direct QZ algorithm is used in order to recover the full eigenspectrum at a cost scaling with the cube of the total number of nodes used in the discretization, the bulk of the analyses is performed using Krylov subspace iteration and the (implicitly restarted) Arnoldi method (IRAM). However, it should be noted that the matrix

$$\mathcal{C} = \mathcal{L}^{-1}\mathcal{R}$$

discretizing the EVP may be formed and kept in memory, in single-domain computations. This is not anymore the case in the multidomain solutions of the EVP, as will be discussed in Section IV.6.

Figure 2: Schematic representation of the possible numerical procedures for the solution of the BiGlobal EVP.

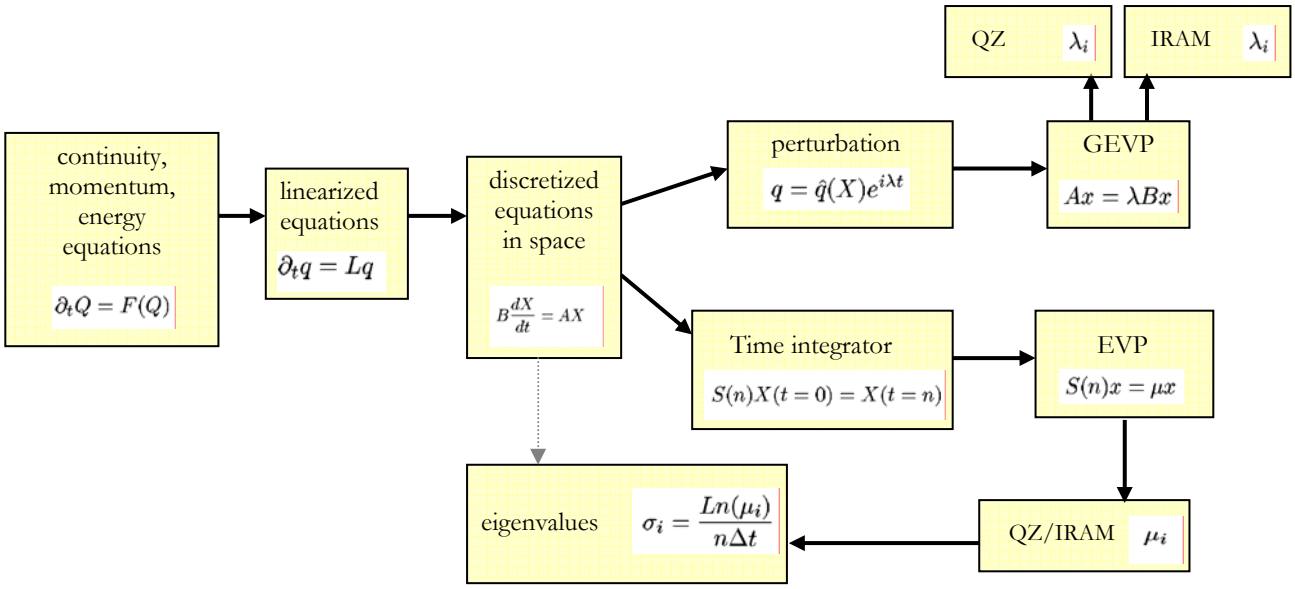

2. The compressible residuals algorithm

The algorithm rests on the identification of small-amplitude residuals in the (unsteady) DNS calculation for the recovery of a steady state as the least damped global two-dimensional eigenmodes of this underlying steady flow (http://handle.dtic.mil/100.2/ADA379181). Concretely, referring to Table 1, the pertinent decomposition is that of BiGlobal theory in the limit of β=0. It is then possible to utilize this information in order to recover the converged steady-state solution as well as the amplitude functions of the least-damped eigenmode from transient data, without having to pursue the time integration of the equations of motion until convergence of the flow in time is obtained.

Consider a transient solution **q** of the equations of motion near convergence to the respective steady state, denoted by the barred quantity, as containing a small-amplitude two-dimensional disturbance according to:

$$\mathbf{q}(x,y,t) = \bar{\mathbf{q}}(x,y) + \varepsilon\ \tilde{\mathbf{q}}_{2D}(x,y,t),$$

where

$$\tilde{\mathbf{q}}_{2D}(x,y,t) = \hat{\mathbf{q}}_{2D}(x,y)\ \mathrm{e}^{\sigma t}$$

Combining this expression with the BiGlobal theory Ansatz shown in Table 1, one obtains

$$\mathbf{q}(x,y,t) = \bar{\mathbf{q}}(x,y) + \varepsilon\ \left[\hat{\mathbf{q}}_\mathrm{r}\cos\omega_\mathrm{r}t - \hat{\mathbf{q}}_\mathrm{i}\sin\omega_\mathrm{r}t\right]\ \mathrm{e}^{\sigma t},$$

where σ may be defined from

$$\sigma = \ln[\mathbf{q}^t/\mathbf{q}^{t-\Delta t}]/\Delta t \approx \mathrm{d}\ln[\mathbf{q}^t]/\mathrm{d}t,$$

with

$$\mathbf{q}^t = |\mathbf{q}(x_0, y_0, t) - \bar{\mathbf{q}}(x_0, y_0)|.$$

The calculation of the basic state and the amplitude functions from transient data follows in two stages. First, elementary signal analysis techniques deliver the results for the circular frequency ω_r. The circular frequency is calculated from the period of oscillations in the transient time-signal of $\mathbf{q}$ which, in turn, is identified by the maxima in the signal. Second, once both ω_r and σ have converged in time, the BiGlobal Ansatz may be used to calculate both the steady basic state and the amplitude functions of the least-damped (β=0)-eigenmode.

Two independent paths may be used in order to calculate σ, depending on whether the transient signal is oscillatory or not. In the first case, the equation

$$\frac{\partial^3 \mathbf{q}}{\partial t^3} + (\sigma^2 + \omega_r^2)\frac{\partial \mathbf{q}}{\partial t} - 2\sigma\frac{\partial^2 \mathbf{q}}{\partial t^2} = 0.$$

may be used, with ω_r. and the time-derivatives known. This expression may be evaluated at those times that the first time-derivative of the signal is zero in the course of the time-integration, i.e. at the same times that ω_r is calculated. At these times the magnitude of σ is given by

$$\sigma = \frac{1}{2}\frac{(\partial^3 \mathbf{q}/\partial t^3)}{(\partial^2 \mathbf{q}/\partial t^2)}\Big|_{(\partial q/\partial t)=0}.$$

On the other hand, in case $\omega_r = 0$, a monotonic dependence of the first time derivative of the signal on time is typically observed from the beginning of the calculation until convergence, with the time-derivative of the signal being zero possibly during early transients and certainly at convergence. Avoiding calculations during the early transient stages, the magnitude of σ may be calculated using

$$\sigma = \frac{(\partial^2 \mathbf{q}/\partial t^2)}{(\partial \mathbf{q}/\partial t)}.$$

With ω_r and σ known, the BiGlobal Ansatz may be written for the case (β=0) as a (complex) linear system of three equations at three times, $t_1 = t$, $t_2 = t + \Delta t$, and $t_3 = t + 2\Delta t$, for three unknowns, namely the steady basic state, and the real and imaginary parts of the amplitude function of the least-damped eigenmode, with the transient solution known at these three times. Simple algebra then delivers the desired converged steady-state solution as

$$\bar{\mathbf{q}} = \frac{\mathbf{q}_1\ e^{2\sigma\Delta t} - 2\ \mathbf{q}_2\ e^{\sigma\Delta t}\cos\omega_r\Delta t + \mathbf{q}_3}{e^{2\sigma\Delta t} - 2\ e^{\sigma\Delta t}\cos\omega_r\Delta t + 1}.$$

With the steady-state solution known, the amplitude function of the least-damped eigenmode may be recovered from

$$\hat{q}_r = \frac{s_1(q_2 - \bar{q}) - s_2(q_1 - \bar{q})}{c_2 s_1 - c_1 s_2}$$

$$\hat{q}_i = \frac{c_1(q_2 - \bar{q}) - c_2(q_1 - \bar{q})}{c_2 s_1 - c_1 s_2},$$

where

$$\begin{aligned} c_1 &= \exp \sigma t_1 \cos \omega_r t_1 \\ c_2 &= \exp \sigma t_2 \cos \omega_r t_2 \\ s_1 &= \exp \sigma t_1 \sin \omega_r t_1 \\ s_2 &= \exp \sigma t_2 \sin \omega_r t_2. \end{aligned}$$

The accuracy of the results delivered by the residuals algorithm clearly depends on that by which the circular frequency and the damping rate are provided, which, in turn depends on the accuracy by which the first three time-derivatives of the transient solution are calculated. The latter is a function of the time-step in the calculation and the number of fields stored, in order for backward differentiation formulae to be applied. Since the time-step is controlled by CFL considerations, it is advisable to store a reasonably high number of fields in order for high accuracy of ω_r and σ to be obtained.

3. A spectral multi-domain algorithm for the BiGlobal EVP in complex cavity configurations

As mentioned, the residuals algorithm was made available to the collaborative Caltech research and has been used a good part of their investigations. The present effort was then diverted toward direct solution of the BiGlobal EVP, for both the (empty) open cavity and full-bay models. In the latter case, a new multi-domain algorithm was designed, validated and applied to various open cavity configurations, as discussed in detail in Section IV. Here the essential aspects of spatial discretization are exposed. For ease of presentation, the incompressible flow limit is considered, where the BiGlobal EVP reads

$$(LHS)U = \lambda (RHS)U,$$

with

$$U = \begin{Bmatrix} \hat{u} \\ \hat{v} \\ \hat{w} \\ \hat{p} \end{Bmatrix}; \; LHS = \begin{pmatrix} L_2 - (D_x(\bar{u})) & -D_y(\bar{u}) & 0 & -D_x \\ -D_x(\bar{v}) & L_2 - (D_y(\bar{v})) & 0 & -D_y \\ 0 & 0 & L_2 & -\beta \cdot I \\ D_x & D_y & -\beta \cdot I & 0 \end{pmatrix}; \; RHS = \begin{pmatrix} I & 0 & 0 & 0 \\ 0 & I & 0 & 0 \\ 0 & 0 & I & 0 \\ 0 & 0 & 0 & 0 \end{pmatrix}$$

Here

$$L_2 \equiv \frac{1}{\mathrm{Re}}\left(D_x^2 + D_y^2 - \beta^2\right) - \bar{u}\,D_x - \bar{v}\,D_y$$

barred and hatted quantities denote basic and disturbance flow quantities, respectively, and D_i denotes differentiation w.r.t. the i-th spatial dimension. Multi-domain resolution, schematically depicted in Figure 3, involves an extended linear system as follows:

Figure 3: Multi-domain spatial discretization of a square domain by two rectangular sub-domains, denoted "green" and "red".

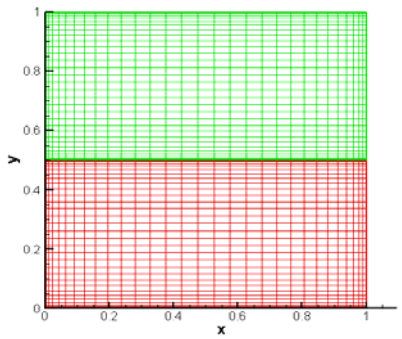

$$LHS = \begin{pmatrix} & & & & CI(\hat{u}) & 0 & 0 & 0 \\ & & & & 0 & CI(\hat{v}) & 0 & 0 \\ & LHS_{red} & & & 0 & 0 & CI(\hat{w}) & 0 \\ & & & & 0 & 0 & 0 & CI(\hat{p}) \\ CI(\hat{u}_y) & 0 & 0 & 0 & & & & \\ 0 & CI(\hat{v}_y) & 0 & 0 & & LHS_{green} & & \\ 0 & 0 & CI(\hat{w}_y) & 0 & & & & \\ 0 & 0 & 0 & CI(\hat{p}_y) & & & & \end{pmatrix}$$

where LHS_{red} and LHS_{green} are linear operators of the same structure as that describing the single-domain BiGlobal EVP solution and CI denotes compatibility conditions at interfaces, necessary in order to couple the two-dimensional amplitude functions of the eigenmodes in the different domains. From the layout of the multi-domain matrix LHS it becomes evident that the direct methods used for the residual matrix operations (matrix factorization, matrix-vector multiplication) in the work of Theofilis *et al.* (2004) become increasingly inappropriate for the solution of the spectral multi-domain problem as the number of sub-domains increases. The reason is that the leading dimension of the multi-domain matrix LHS is a multiple of that of the single-domain matrices (already very large) LHS_{red} and LHS_{green}. Consequently, particular efforts were devoted toward efficient solutions of the multi-domain EVP, the details of which are provided in Section IV.

IV. TECHNICAL RESULTS

1. Computing cluster installation and performance

In preparation for the execution of the project, computing hardware has been acquired, according to the provisions of the Grant. Such hardware corresponds to an 8-node cluster (16 processors/16Gbytes), as originally planned. However, the drop in prices between the time at which the Grant has been approved and that of the hardware acquisition has resulted in the ability to purchase a fast (Myrinet) inter-nodal connection hardware, to ensure rapid communication of data in the invariably parallel computations within the project, in both the direct numerical simulations - DNS and the BiGlobal stability analysis aspects of the work. Furthermore, rather than investing in a stand-alone cluster facility, the hardware configuration acquired was chosen to be compatible with a newly-built computing cluster facility at the Universidad Politécnica de Madrid (UPM), the academic affiliation of Theofilis. This cluster currently comprises a total of 64 nodes (128 processors/256 Gbytes) and there exist 15 Tbytes of storage space. The cluster runs under Linux, parallelization is done using MPICH and PBS is used as job-scheduling software. The decision to invest in compatible hardware was taken with the objective in mind to maximize the computing power available to *nu-modelling,* beyond the 8-node configuration pertaining to the company. The modus operandi during the execution of the Grant has been that, when the 8-nodes pertaining to *nu-modelling* were not needed in their entirety (e.g. during code-development phases), they have been used by other UPM members. In exchange, when production-runs associated with the Grant have been necessary, *nu-modelling* had access to a computing facility that is substantially larger than that owned by the company. The decision to spend a substantial portion of the funds set aside for computing hardware in inter-nodal connection hardware, as opposed to a larger number of processors, has been taken on grounds of hardware performance, as explained next.

Commensurate with the first objective of the first phase of the Grant, the (MPICH-) parallelized 2d-DNS code of Caltech has been ported on this, as well as predecessors of the aforementioned cluster. Speed-up factors have been realized when using the ("new") cluster, compared with performance on a machine available at UPM prior to this cluster, designated as "old" in what follows. Speed-up has been realized commensurate with two factors, the processor and the communication speed. Table 2 shows a comparative study of performance of the same version of the DNS code. Shown are the processor type, **Proc,** the time spent while computing, $\mathbf{t_{CPU}}$, and the time spent in data-exchange (communication), $\mathbf{t_{COM}}$, both in seconds per step in the code, the actual (as opposed to theoretical) sum of these two times, $\mathbf{t_{STEP}}$, in seconds and the ratio $\mathbf{t_{COM} / t_{STEP}}$, indicating the percentage of time spent communicating data, as opposed to computing. In order to facilitate comparisons, the same number of 20 processors has been used on both the "old" and the "new" clusters. Both machines use fast inter-node connection (Scali in the "old" and Myrinet in the "new" cluster). For this moderate computation the speed-up realized on the "new" machine is due to both its faster processor type and its faster inter-nodal connection hardware.

Table 2: Comparative study of code performance on the two clusters.

Cluster	Proc (GHz)	t_{CPU} (s/STEP)	t_{COM} (s/STEP)	t_{STEP} (s)	t_{COM} / t_{STEP} (%)
"old"	P-III (1.8)	64.23	18.60	88.4	21
"new"	P-IV (3.06)	45.97	8.97	57.7	15

The situation changed, as the computation became more demanding and a larger number of processors and memory were necessary. The speed-up factor in this case turned out to be determined by communication-, rather than calculation-speed. Figure 4 shows the speed-up factor, this time measured in terms of number of steps realized by the DNS code per second (**S/sec**) as the number of processors (**np**) increases. For this comparison the "new" cluster has been used, communicating data either through its Gigabit network (used for NFS operations) or through its Myrinet network (used for computations). It may clearly be seen that both solutions performed comparably well at low number of processors; however, as **np** increased, the Myrinet-based computation scaled perfectly linearly, i.e. *the number of time-steps calculated increased linearly with the number of processors used*. On the other hand, past a threshold, *the Ethernet-based solution reached a plateau of number of time-steps computed, irrespective of the number of processors used*. In other words, an Ethernet-based solution would have become a bottleneck for large-scale computations, of the type actually performed later, for both three-dimensional multi-domain BiGlobal instability analysis and DNS. With hindsight, this has justified the decision to balance the expenditure of the funds made available within the scope of the Grant between number of nodes and (expensive but fast) inter-nodal connection Myrinet hardware.

Figure 4: Comparative study of code performance on an Ethernet-based (dotted line) and a Myrinet-based (solid line) cluster.

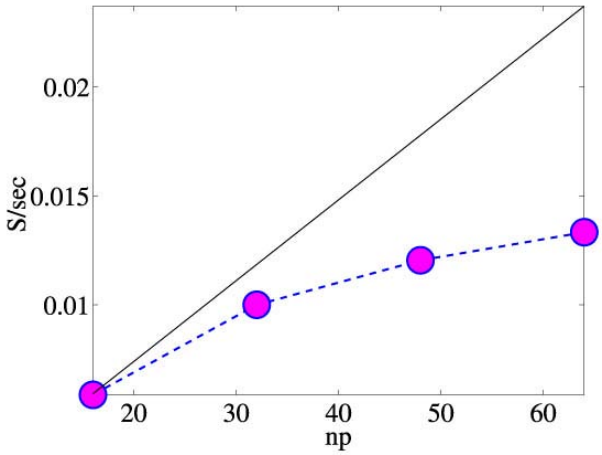

A parallel development, unforeseen at the time of application of the grant, has been relevant to the Grant execution, namely the installation of two large supercomputer facilities in Spain. *Mare Nostrum* has been installed in the Barcelona Supercomputing Center, while its smaller counterpart, *CeSViMa* (Centro de Supercomputación y Visualización de Madrid) has been installed at (and owned by) the Universidad Politécnica de Madrid; they are both IBM Linux clusters, respectively featuring ~4k and ~1k processors interconnected by Myrinet hardware. The existence of the first of these machines has overlapped the longest with the duration of the Grant but has been under testing throughout the entire same period, so that no access to it was requested. The local supercomputer has been utilized toward the end of the Grant, in order to clarify parallel performance issues with respect to the sparse-matrix solution algorithms used in the spectral multi-domain solution of the BiGlobal EVP. It was shown that no gains are to be expected by performing the analysis related with the Grant on a supercomputer, such that for the bulk of the analyses reported below, the numerical work has been executed on the local UPM cluster described above.

2. First application of the compressible residuals algorithm in compressible flow

At the beginning of the Grant execution, the connection with previously-initiated global instability analysis research was made by applying for the first time to a compressible flow instability problem the "residuals" algorithm devised by Theofilis during EOARD-sponsored work (F61775-99-W-E090 http://handle.dtic.mil/100.2/ADA379181) for incompressible flows. This algorithm may be used in conjunction with two- or three-dimensional DNS in order to recover the underlying instability characteristics of the flow from transient DNS data. Prior to the Grant, the algorithm had only been applied to incompressible flows while during the Grant, and in collaboration with the Caltech team, the algorithm has been applied for the first time to compressible DNS data, as discussed below.

Technical details of the residuals algorithm were presented in the Section III.2. In brief, the residuals algorithm uses simple algebraic operations on unsteady DNS data and delivers both the steady-state and the instability characteristics of any (one-, two-, or three-dimensional) flow from unsteady DNS data, the latter taken during the early stages of the integration time necessary to reach convergence. The alternatively available methodology in order for instability results to be obtained is to march the unsteady DNS until convergence to a steady-state and subsequently solve the appropriate corresponding (one-, two- or three-dimensional) eigenvalue problem (EVP). It is known that the cost of the DNS scales with the powers 6/4 and 9/4 of Reynolds number in two- and three-spatial directions, respectively. Moreover, as discussed by Theofilis (2003), the leading dimensions of the matrices involved in the solution of the BiGlobal and TriGlobal EVP scale with the product of the degrees of freedom used to resolve two- or three spatial directions, respectively, such that the residuals algorithm permits recovery of the sought instability results at an insignificantly small fraction of the otherwise necessary computing effort. An example of successful application of the algorithm on the classic lid-driven cavity problem is shown in Table 3 and the associated Figure 5. Single overbar denotes time at which the DNS solution converges, while double overbar denotes time at which the residuals algorithm was applied; in all cases the latter is of O(20%) of the former time, indicating the substantial savings achieved. The shorthand notation

$$\Delta\overline{\overline{\mathbf{q}}} \equiv |(\overline{\overline{\mathbf{q}}} - \bar{\mathbf{q}})/\bar{\mathbf{q}}|$$

denotes the relative error between quantity q evaluated at the aforementioned early time over the respective converged-in-time quantity, the latter obtained at the end of the time integration.

Table 3: Recovery of the stream function ψ in the square liddriven cavity problem, from transient DNS data taken at time t=20, out of a time-to-convergence being t=100. The effect of resolution and timestep used in the DNS is examined at Re=100; $x(y) \equiv x \times 10^{y}$ (Theofilis and Colonius 2003).

DNS Run	I	II	III
Resolution	16×16	24×24	32×32
Δt	0.01	0.01	0.005
$\bar{t}$	50.43	50.42	49.005
$\bar{\bar{t}}$	12.71	12.79	11.07
$-\sigma$	0.540246	0.540214	0.540876
$\max(\Delta\bar{\bar{\psi}})$	5.3(−8)	8.8(−7)	4.6(−6)
$\min(\Delta\bar{\bar{\psi}})$	3.6(−9)	7.9(−8)	5.1(−7)
$\max(\Delta\psi)$	3.4(−4)	3.5(−4)	1.0(−3)
$\min(\Delta\psi)$	1.5(−5)	1.2(−3)	1.6(−2)

Figure 5: Left: The approximation for ψ(x, y; t = 20) obtained from application of (14) to transient DNS data at Re = 100 and t = 20. Right: The spatial distribution of the approximation error.

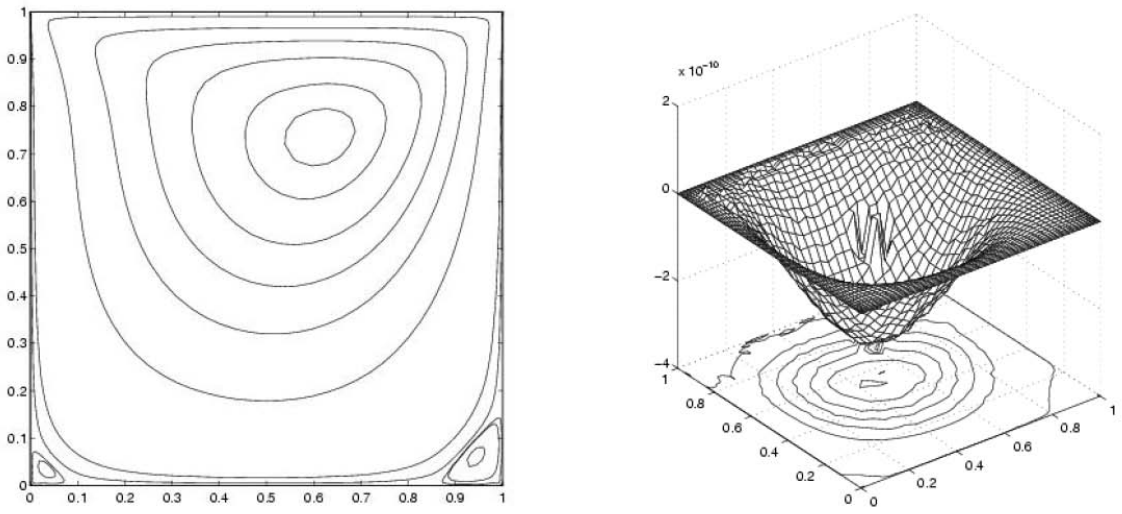

The most significant results here are (i) the low level of approximation error max(Δψ) and (ii) the ratio of the ("double-overbar") time at which the transient solution is processed to that ("overbar") otherwise necessary for the DNS to converge. The case Re = 100 is typical of one in which the least stable eigenmode determines the transient behavior of the DNS throughout most of the time integration process. With the results for the damping rate σ converging quite quickly, the desired converged steady state may be obtained at a time between a quarter at the coarsest and a fifth at the finest resolution of the time required by the time - marching algorithm for the residuals to be eliminated. The result for σ is only marginally affected by resolution and time step; the precise times at which σ converges are affected by a small amount when refining the grid, with the finest resolution results converging earlier. In all cases application of the residuals algorithm results in substantial savings compared with the otherwise necessary computing effort.

Table 4 Parameters of compressible open cavity L/D=2 DNS runs performed.

DNS Run	I	II
Re_θ	56.9	91.0
Re_D	1500	2667
Ma	0.2	0.8

The first application of the residuals algorithm to compressible flows was presented by Theofilis and Colonius (2003). The well-validated high-order DNS methodology of Caltech has been used for the recovery of the basic states that were analyzed, while the residuals algorithm was derived and coded in a joint effort of the *nu modelling* and Caltech teams. Basic flow results of two simulations, the parameters of which are summarized in Table 4, have been isolated for some discussion here, owing to their representative nature. The time-dependence of the normal velocity component at a single location inside the cavity, shown in Figure 6, is characteristic of the signal returned by the DNS I for any flow quantity. Such a signal is composed of

two damping BiGlobal eigenmodes, a traveling one visible in the signal during $t \in [0, 300]$ and a stationary one, which emerges (although damped throughout the time-integration) beyond $t > 300$. Before discussing the characteristics of the BiGlobal instability eigenmodes, the residuals algorithm has first been employed in order to recover the steady state towards which the solution is converging. Owing to the presence of multiple modes in the simulation, a relatively long time-integration has been necessary before the residuals algorithm could be applied. Nevertheless, the comparison of the estimated and the exact steady states revealed approximation errors of 10^{-10}, in line with the analogous result in the lid-driven cavity flow.

Figure 6: Time development of the normal velocity component in DNS I

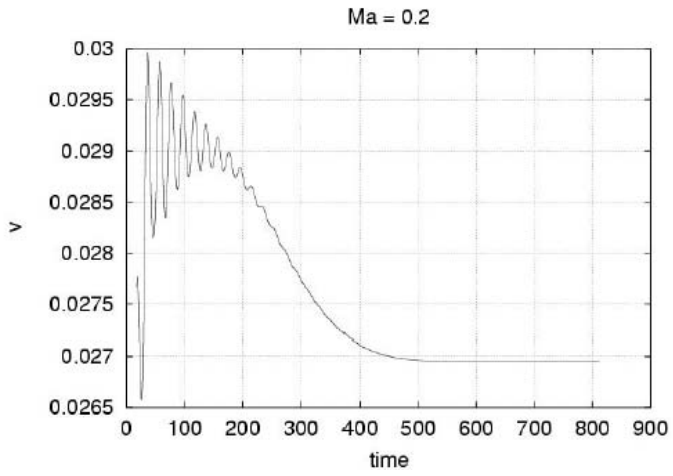

Turning to the spatial structure of the BiGlobal eigenmodes being damped in the DNS process, Figures 7 and 8 show the real and imaginary parts of the complex amplitude functions corresponding to the wall-normal disturbance velocity and the disturbance pressure, as obtained at $t = 100$ and 600, respectively. At $t = 100$ the traveling eigenmode is dominated by a Tollmien-Schlichting wave developing along the downstream cavity wall and being damped in time. At $t = 600$ this mode has subsided and the only remaining disturbance is a stationary mode, which needs to be damped before the steady-state solution is obtained.

Three properties of this mode, its being stationary, its scaling with a geometric length scale of the cavity, and its location inside the open cavity point to this BiGlobal eigendisturbance being related with the wake-mode of Gharib and Roshko (1987). On the other hand, the spatial structure of the amplifying eigenmode manifesting itself in a linear manner at early times during DNS II has a distinctly different spatial structure of the amplitude functions. Figure 9 also shows the same quantities as presented in Figures 7 and 8; in both results one may notice the following features. First, the dominant structure is located at the open end of the cavity and appears to be related with instability in the shear-layer, of the class predicted by the Rossiter analysis. Clearly, this disturbance is only part of the amplitude function, a significant part of which may be identified as a Tollmien-Schlichting wave on the downstream wall of the open cavity. Furthermore, acoustic pressure disturbances may be identified in the respective amplitude function, apparently originating at the downstream corner of the cavity and propagating upstream in the field. The acoustic disturbances are weak in comparison with the maxima of their respective hydrodynamic counterparts. The most interesting aspect of these results is that **all instability features, which have received attention independently in the past, are part of one and the same BiGlobal flow eigenmode**.

Figure 7: Real- and imaginary parts of the wall-normal complex disturbance velocity component (upper row) and pressure perturbation (lower row) in DNS I at t=100

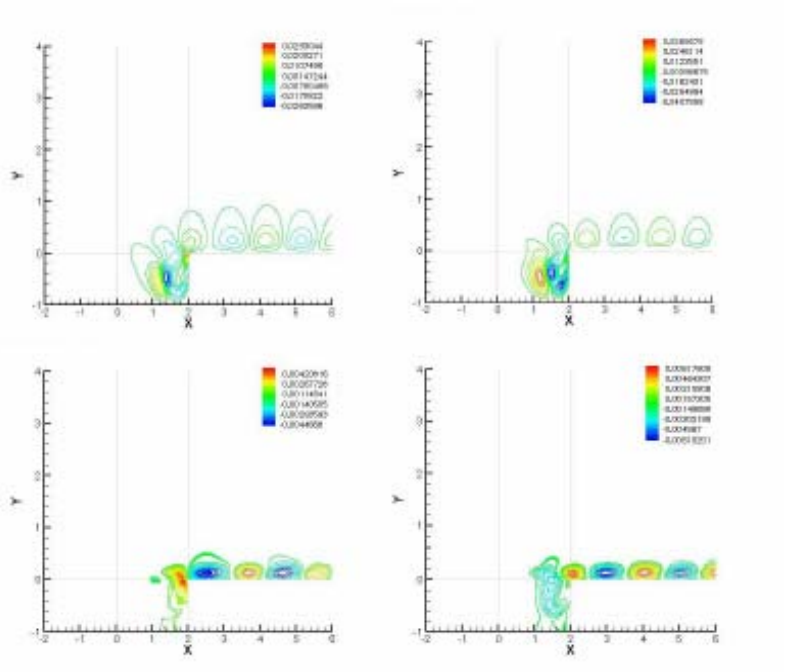

Figure 8: Same as in figure 7, at t=600

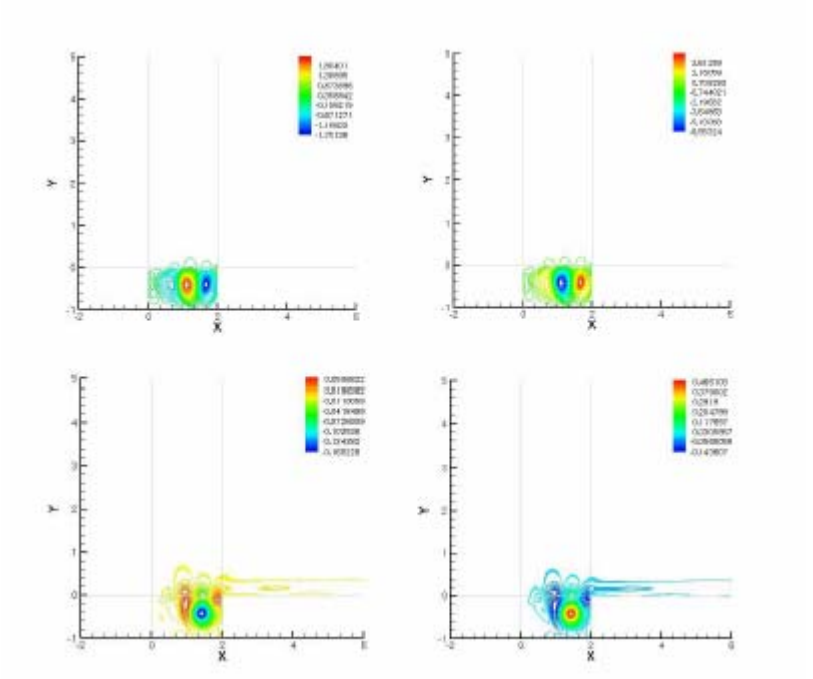

Figure 9: Same as in figure 8, for DNS II

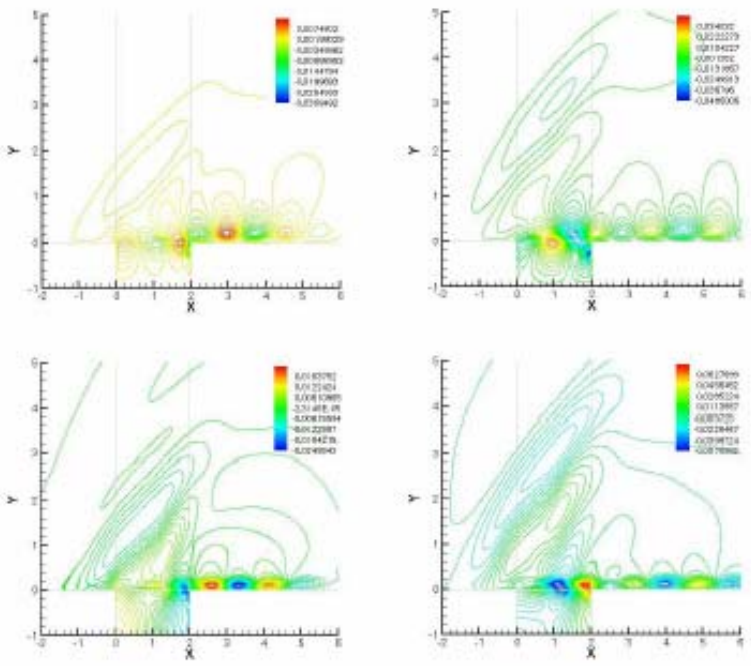

3. Classes of instability modes discovered: a unifying perspective

The first application of the residuals algorithm for the recovery of BiGlobal instability results from DNS data to the compressible open-cavity flow problem has yielded the spatial structure of the most energetic members of the BiGlobal eigenspectrum, that are otherwise accessible to numerically challenging solutions of the partial-derivative eigenvalue problem, or to DNS. The present, and analogous results not presented here, have permitted forming a unified point of view of open cavity flow instabilities. Known shear-layer (Kelvin-Helmholtz – KH), Tollmien-Schlichting (TS) or newly-discovered (wake-mode-related) hydrodynamic and aeroacoustic **instabilities** in open cavities have been shown to **emerge as components of the amplitude function of single BiGlobal eigenmodes.** This re-interpretation is broader than previously used modeling approaches in an essential manner, namely in that it permits addressing the **nonparallel** open cavity flow instability problem in its entirety, rather than focusing on one, or some of its features (such as the shear-layer, the downstream TS mode or the acoustic wave emanating from a corner) in isolation from the rest of the flow. The presently offered framework opens new modeling avenues for such instabilities. In line with two of the objectives of the Grant, this result has provided a novel framework for classification and a unified perspective of all cavity instabilities. A systematic study of this point was continued in the framework of the related Caltech effort. At *nu modeling*, results obtained to this point underlined the necessity to develop a new compressible BiGlobal eigenvalue problem solver, in order to aid the study of open cavity flow disturbances with an essentially inhomogeneous nature, such as the wake-mode instability outlined above.

4. On the role of three-dimensionality in the cavity

Prior to embarking upon new developments towards satisfying the next objective of the Grant, namely advance the current understanding of the role of three-dimensionality in cavity instability, an incompressible model of three-dimensional cavity flow has been devised and analysed using BiGlobal instability analysis. The reason for introduction of this model has been that, while on occasion BiGlobal instability analysis delivers results in excellent agreement with experiment (e.g. Theofilis 2000 – EOARD-sponsored research F61775-99-W-E090) there exist anomalies in the predictions of linear (both classical 1D and BiGlobal) theory. Most notable of these anomalies, explainable within the framework of transient growth theory (Schmid and Henningson (2001), is the failure of 1D linear theory to predict instability in Hagen-Poiseuille (pipe) flow, aggravated by the erroneous predictions of BiGlobal theory of stability of pressure-gradient driven flow in a square duct (Tatsumi and Yoshimura 1990) and wall-bounded Couette flow. It thus becomes of interest, before investing efforts in the development of a new compressible BiGlobal EVP solver in an open cavity configuration, to provide (even partial) answers to the question whether application of Bi-/TriGlobal linear theory to the open cavity is expected to deliver realistic results. Resolution of this issue has been particularly pressing at that stage of the Grant, since the conclusions reached on the aforementioned question would determine the direction which the project should take from that point on. The two alternatives would be to focus on the numerical solution of the eigenvalue problem or pose the problem of stability in the open cavity in the broader context of solutions of (linear) initial value problems. The latter option would permit addressing the issue of transient growth at short times and that of eigenmodes at the limit of large times of the same analysis. However, the cost of performing a transient-growth study, in addition to the essential change of focus in the Grant objectives, would require strong justification. It turned out that linear theory in the form of BiGlobal analyses delivered unstable eigenvalues in the model three-dimensional problem and, as such, the original plan was pursued.

Figure 10 illustrates the configuration chosen in order to address the question of three-dimensional instability and relevance of BiGlobal theory in the model problem. Motion of a lid at an arbitrary angle ϕ sets up a three-component basic flow inside the cavity, the limiting cases of which are the classic lid-driven cavity (at $\phi = 0$, where BiGlobal theory predicts excellent agreement with experiment; Theofilis 2000), and the wall-bounded Couette flow at $\phi = \pi / 2$ which is (erroneously predicted by BiGlobal analysis to be) stable. The introduction of a third velocity component by the lid-motion along the homogeneous direction results in an order-of-magnitude increase of the computing effort in order to solve the BiGlobal EVP; however, reliable solutions to this problem can be obtained using a purpose-built extension of a well-validated incompressible BiGlobal EVP solver (Theofilis, Fedorov, Obrist and Dallmann 2003). Results obtained in the 3D cavity model at all intermediate ϕ –values, shown in Figure 11, demonstrate that **the known modes of the lid-driven cavity S, T1, T2 and T3 persist in the case of three-dimensional flow**. Three-dimensionality was found to be essential in introducing linear amplification; at the low Reynolds number examined, at which steady two-dimensional states were predicted by 2d DNS, instability appears in the flow on account of $\beta = 2\pi/L_z \neq 0$, L_z being the finite spanwise extent of the cavity. The levels of (viscous) amplification ($\omega_i > 0$) are analogous to those of the lid-driven cavity, which in turn agree very well with experiment. It was further discovered that the range of amplified frequencies, denoted by ω_r in Figure 11, is a function of the angle considered, being widest at the cavity-related limit. It thus appears that the wall-bounded Couette flow is a singular exception, due to the absence of velocity components on the plane normal to the wavenumber vector. This result builds confidence in employing BiGlobal analysis to the three-dimensional compressible open cavity linear instability problem.

A major publication (Theofilis, Duck and Owen 2004) has thus been generated during the first year of the Grant. Material has been composed of (a) BiGlobal instability results in rectangular duct and wall-bounded Couette flow, performed prior to this grant in collaboration with Prof. P. W. Duck and his student Mr. J. Owen of Manchester University, UK, (b) EOARD-supported research of Theofilis in the lid-driven cavity (contract F61775-99-WE090) and (c) a subset of the results obtained by *nu modelling* in the first year of the present grant. Based on the Referees' report it is clear that the inclusion of the model-cavity results in (c) has been instrumental in the acceptance of the paper for publication.

Figure 10: A model three-dimensional flow in cavities (Theofilis, Duck & Owen *J. Fluid Mech.* **505**, 249-286, 2004).

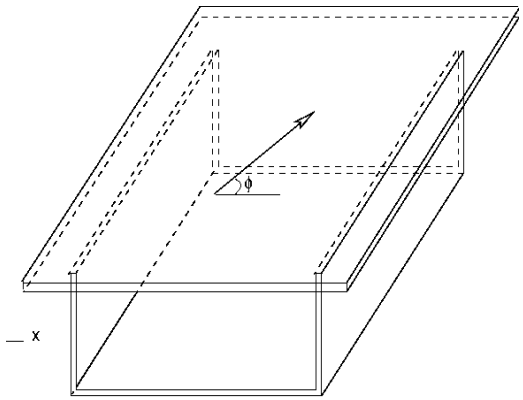

Figure 11: Dependence of amplification rates on wavenumber in (*a*) and frequency in (*b*) at three angles $\phi = \pi / 8$, $\phi = \pi / 4$ and $\phi = 3\pi / 8$ and two Reynolds numbers Re =900 (dotted line) and 1000 (solid line) (Theofilis, Duck & Owen *J. Fluid Mech.* **505**, 249-286, 2004).

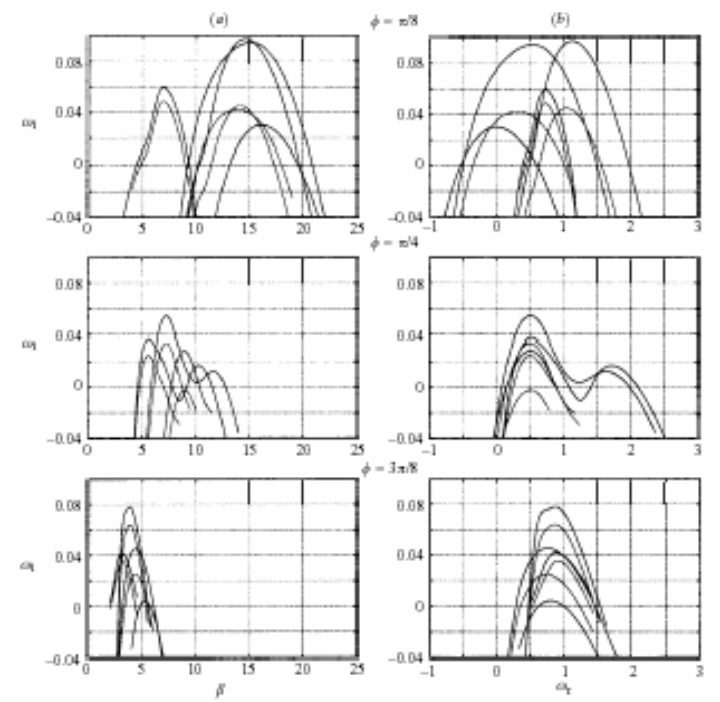

5. Direct solution of the compressible BiGlobal eigenvalue problem

Motivated by the need to further understand whether and how three-dimensionality changes the transition boundaries between shear layer and wake mode, a new compressible BiGlobal EVP solver has subsequently been designed, hard-coded and validated at *nu modelling*. Design characteristics of the code have been a) high-accuracy, b) flexibility in terms of both the complexity of the geometry addressed and general constitutive laws admitted by the code (equation of state, viscosity dependence on temperature, the latter permitting us to address flow instability up to the hypersonic regime) and, c) completeness and efficiency in the computation of the eigenspectrum. In the first implementation of the code, steps taken towards meeting the aforementioned characteristics have been the use of a) single-domain spectral collocation methods on a two-dimensional staggered Chebyshev Gauss-Lobatto/Gauss grid, later to be extended by spectral-multidomain or spectral-element techniques (Theofilis EOARD Final Report F61775-01-WE049), while b) a perfect-gas law and c) the QZ algorithm for the recovery of the entire eigenspectrum completed the initial implementation.

An essential aspect of every new development is careful validation against well-established results. The compressible BiGlobal EVP as defined here describes small-amplitude perturbations superimposed upon an *arbitrary two-dimensional* basic state. In the limiting case of such a basic state being a one-dimensional profile (e.g. those pertaining to the boundary-layer or shear-layer, both of which are directly relevant to the cavity problem at specific locations in the cavity) the BiGlobal *two-dimensional* EVP reduces to the well-known *one-dimensional* EVP. The latter EVP has been utilized to perform exhaustive investigations into the stability of compressible flat-plate and axisymmetric boundary-layer and shear-layer flows over the span of several decades (Mack 1984). The newly-developed, more general, code has been validated thoroughly against such results, since the latter form the cornerstone of practically all current analysis and control methodologies of flow in the open cavity that are based on flow instability.

Results are presented, beginning with cases that serve to validate the numerical method and illustrate our approach. These include an incompressible square duct, the flat-plate boundary layer from incompressible speed to Mach number, $Ma = 6$ flow, and an isolated parallel two-dimensional shear layer. Excellent agreement with the results of Mack (1984) has been obtained; as an example, components (amplitude functions of disturbance velocity and disturbance temperature) of the (one-dimensional) eigenvector pertaining to three-dimensional instability of a Ma=6 flat-plate boundary layer are shown in Figure 12. The complex structure of these perturbations and the characteristic of compressible flow critical layer (i.e. the location where the phase velocity of the instability wave equals that of the basic state, located at a wall-normal distance $y \approx 20$ at these parameters) can clearly be seen in these results. Results are presented on the collocation grid used, in order for the resolution requirements in the cavity problem to be appreciated: the grids shown are the one-dimensional restrictions of a two-dimensional BiGlobal instability analysis grid that would be necessary in order to recover these instabilities at the same level of accuracy. The amplification rates of linearly unstable compressible flow over a flat plate, accurate to all significant digits presented, are shown in Table 5; those pertinent to compressible shear-layer flow, alongside comparisons against earlier works, are shown in Table 6.

Figure 12: Streamwise and spanwise disturbance velocity components and temperature perturbations on a flat-plate boundary layer at *Ma* = 6 (Theofilis and Colonius AIAA 2004-2544).

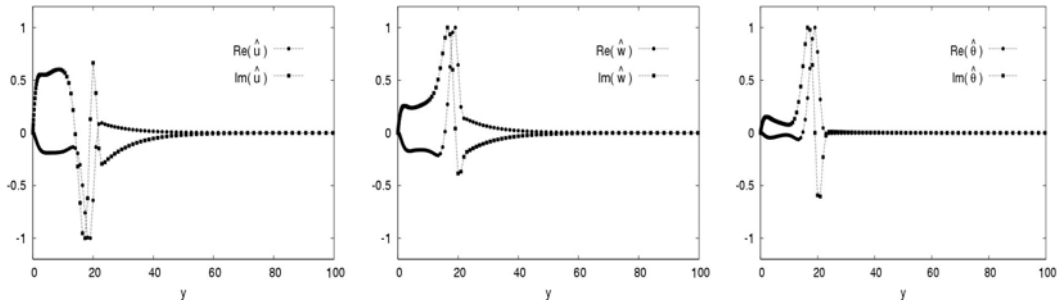

In Table 5 Ma denotes Mach number, δ^* is the displacement thickness of the similarity solution of the compressible flat-plate boundary layer solution in multiples of a unit length, Re_{δ^*} is the associated Reynolds number, α, β are wavenumber parameters of three-dimensional Tollmien-Schlichting instability waves, ψ the associated angle (in radians) and (ω_r , ω_i) the computed eigenvalue. The same symbols are used to describe two-dimensional (β=0) shear-layer instability in Table 6. Note that the latter inviscid instability results have been obtained by setting a large Reynolds number value, $Re = 10^4$, in our code.

Table 5: Validation of the compressible BiGlobal EVP solver on the compressible flat plate boundary layer instability

Ma	Re_{δ^*}	δ^*	α	$\psi = \text{atan}(\beta/\alpha)$	(ω_r , ω_i)
10^{-3}	800	1.720788	0.12	30	(0.040583234, 0.001728706)
1	1000	2.004500	0.10	45	(0.038017729, 0.001350618)
6	1000	17.696682	0.08	45	(0.072487839, 0.001052149)

Table 6: Validation of the compressible BiGlobal EVP solver on the compressible shear layer instability

Ma	α	Blumen	Macaraeg et al.	Present results
0.0	0.445	0.190	0.18954	0.189539
0.2	0.426	0.181	0.18112	0.181156
0.4	0.409	0.158	0.15760	0.157581
0.6	0.370	0.122	0.12180	0.121763
0.8	0.279	0.078	0.07760	0.077607

Subsequent work at *nu modelling* has focused on two aspects of the newly-developed compressible BiGlobal eigenvalue problem (EVP) solver. First, validations have continued using analytically-known two-dimensional basic states. Results obtained independently by the established incompressible BiGlobal EVP solver of Theofilis (Theofilis *et al.* 2003; 2004) have been reproduced by the new compressible BiGlobal solver, the latter run at a low Mach number $Ma = O(10^{-4})$. One such comparison is shown in Figure 13, where the excellent agreement between the eigenmodes of rectangular duct flow, as delivered by the two codes can be seen, alongside newly-found instability modes associated with the energy equation; the latter can only be obtained by the new compressible BiGlobal EVP solver.

Figure 13: The BiGlobal eigenspectrum of incompressible rectangular duct flow (Theofilis, Duck & Owen 2004 *J. Fluid Mech.* **505**, 249-286), recovered by the developed compressible BiGlobal EVP solver, using two different two-dimensional staggered spectral collocation grids.

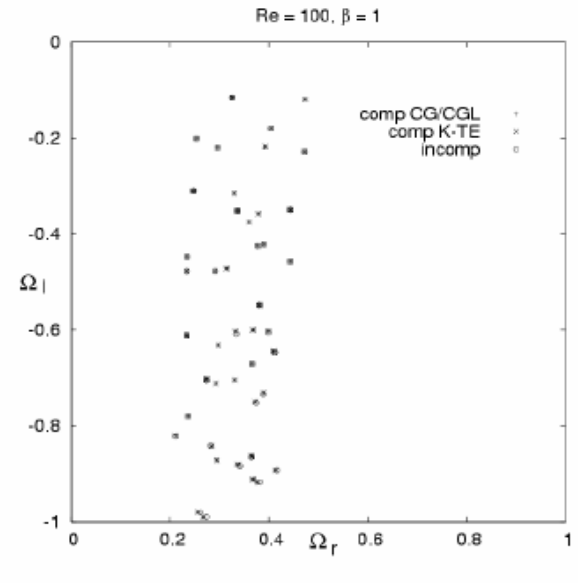

Second, the first-ever BiGlobal instability results of *three-dimensional* compressible open cavity flow have been obtained by *nu modelling*. The steady-state compressible basic flow solution in a L / D = 2 cavity has been produced by 2-D DNS and delivered to *nu modelling* by the Caltech team. The conditions Re = 1500 and Ma = 0.325 were chosen to ensure steadiness of the basic flow. In the BiGlobal EVP solution the streamwise and normal spatial directions defining the open cavity have been resolved in a coupled manner, while the third, spanwise spatial direction has been treated as periodic. The extent of the spanwise domain, L_z, has been determined by a wavenumber parameter $\beta=2\pi/L_z$ and chosen to be unity. First results obtained were focused on the flowfield inside the cavity; at the parameters chosen only stable modes have been recovered. The amplitude functions of the dominant streamwise disturbance velocity components of the two least-damped modes are shown in Figure 14, where the complexity of these structures, as well as their connection with instability mechanisms outside the cavity, can clearly be seen.

Figure 14: The two least-damped BiGlobal eigenmodes of compressible aspect-ratio-2 open cavity flow; streamwise disturbance velocity components of the traveling mode *(left)* and the stationary mode *(right)* (Theofilis and Colonius AIAA 2004-2544)

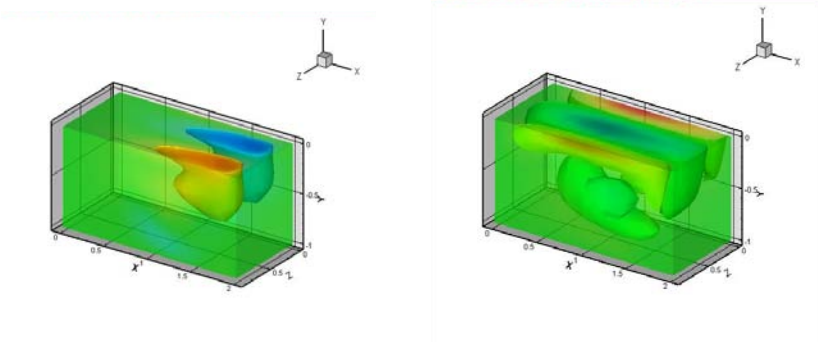

Subsequently, work focused on two aspects of the single-domain compressible BiGlobal EVP solver, namely improving its *efficiency* and *flexibility*. The first improvement was accomplished by implementing an (implicitly restarted) Arnoldi method (IRAM) for the solution of the large partial derivative eigenvalue problem. This algorithm recovers the most significant (most amplified/least damped) part of the eigenspectrum, as opposed to all members of the eigenspectrum that the QZ algorithm delivers, as seen in Figure 15. The advantage of the Arnoldi over the QZ approach (the latter used by Theofilis and Colonius 2004) is that the leading eigenmodes are recovered using O(N) in the former, as opposed to O(N^3) operations in the latter algorithm. N is the leading dimension of the BiGlobal eigenvalue problem matrix, which, in turn, is the product of nodes resolving the two spatial directions times the number of equations solved (five, in the compressible regime). The resolution requirements are a function of the Reynolds number addressed; in typical applications N can be of the order of 10^4, which renders the calculation speed advantage the Arnoldi algorithm over the QZ approach decisive for the success of BiGlobal instability analysis, in a twofold manner.

First, use of the Arnoldi algorithm permits fast recovery of high-resolution results at moderate Reynolds numbers. Alternatively, the Arnoldi algorithm delivers results of moderate (but adequate) resolution substantially faster than the QZ algorithm, which, in turn, facilitates performance of fast parametric studies. Second, use of the Arnoldi algorithm requires storage/manipulation of a single (large) array while the QZ algorithm needs four such arrays to be stored. The memory freed by the Arnoldi algorithm may be devoted in order to address instability problems at high Reynolds number values inaccessible to the QZ algorithm. Using the basic states provided by Caltech the Arnoldi algorithm was employed to extend the computations of Theofilis and Colonius (2004); one result of this effort is shown in Figure 15. The associated amplitude functions of the leading eigenmodes are shown in Figure 16 (using the QZ algorithm) and in Figure 17 (using the IRAM approach). Both results are obtained using the same level of computing effort, explicit matrix formulation and storage, as well as serial computing. The resolution improvement that the Arnoldi algorithm offers may be appreciated by comparing the results of these figures.

Figure 15: The BiGlobal eigenspectrum of compressible two-dimensional open cavity flow obtained using the QZ algorithm (+) by Theofilis and Colonius (2004). Superimposed are shown identical values of the most significant part of the eigenspectrum, as obtained using the Arnoldi algorithm (o).

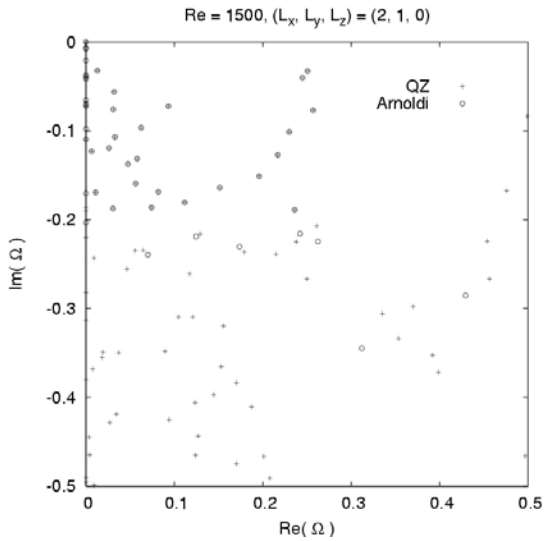

Figure 16: Amplitude functions of the disturbance velocity components of the first traveling ($\Omega_r \neq 0$) and the first stationary ($\Omega_r = 0$) three-dimensional BiGlobal eigenmode at aspect ratio $L_x/D = 2$ compressible open cavity flow at Re = 1500 and Ma = 0.325, corresponding to a narrow spanwise periodicity domain $L_z = 1$, ($\beta = 2\pi/L_z \approx 6.28$).

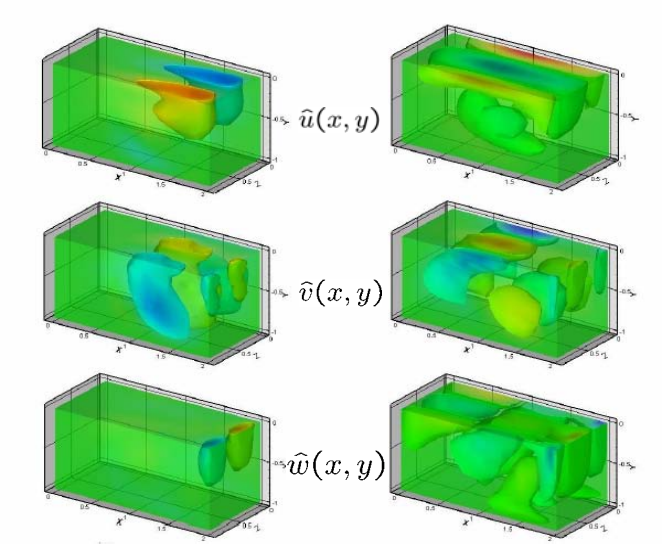

Figure 17: Amplitude functions of the disturbance velocity components of the first traveling ($\Omega_r \neq 0$) and the first stationary ($\Omega_r = 0$) three-dimensional BiGlobal eigenmode at aspect ratio $L_x/D = 2$ compressible open cavity flow at Re = 1500 and Ma = 0.325, corresponding to a wide spanwise periodicity domain $L_z = 2$, ($\beta = 2\pi/L_z \approx 3.14$).

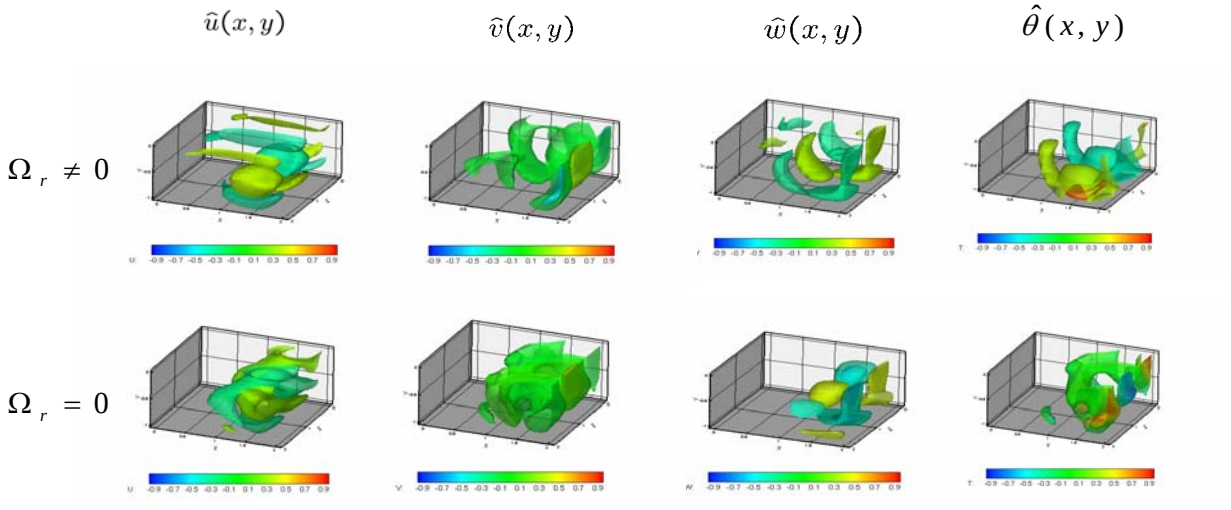

Regarding *flexibility* of the BiGlobal EVP solver, results such as those shown in Figures 16 and 17 were obtained by considering the domain inside the cavity in isolation from the flowfield outside the cavity and imposing homogeneous Neumann boundary conditions in the open end of the domain. Such results were confirmed by the independent Caltech effort; this team has extended their DNS code in order to solve the linearized Navier-Stokes equations and obtained leading eigenmode results in close qualitative agreement with those obtained by the direct solution of the BiGlobal eigenvalue problem; direct quantitative comparisons were not possible since the computational-resources-intensive nature of the linearized Navier-Stokes methodology only permits a modest resolution of the structures delivered by the BiGlobal analysis inside the cavity. Conversely, the BiGlobal methodology at the time of those comparisons was confined to the solution of the eigenvalue problems in single-domains, and resolved the domain inside the cavity, neglecting parts of the eigenmode potentially extending outside the cavity, that were threated by the linearized DNS approach. This provided strong motivation for the developments that followed in the direction of multi-domain solutions of eigenvalue problems, in order to address BiGlobal instability of both the entire cavity domain and complex full-bay configurations.

Figure 18: The streamwise disturbance velocity component of the least-damped BiGlobal eigenmode of compressible aspect-ratio-2 open cavity flow, delivered by the Arnoldi algorithm; in the background the steady laminar basic state upon which this instability develops is shown.

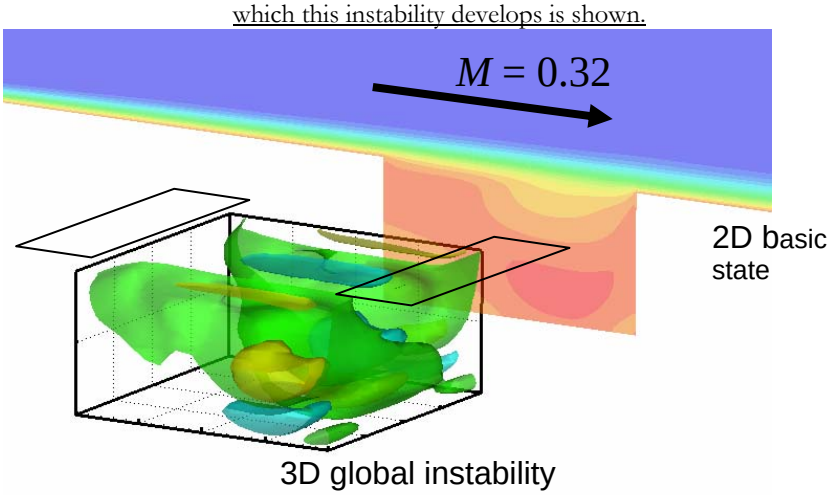

In summary, the direct solutions of the BiGlobal eigenvalue problem obtained in this part of the research have been the first-ever successful solutions of the problem of linear instability in the open cavity, without the need to resort to the strong assumption of parallel flow, as invariably done in previous efforts. As such, structures inaccessible to classic linear analysis of the Kelvin-Helmholtz / Tollmien-Schlichting class have been obtained for the first time, as schematically depicted in Figure 18. With work underway at Caltech, using either the residuals algorithm or the linearized Navier-Stokes approach in order to identify stability boundaries in the multiparametric (empty) open cavity problem, attention was diverted to the issue of a full-bay configuration. As an aside, it is worth mentioning that the new single-domain compressible BiGlobal EVP solver was employed to study another instability problem of long-standing interest, that in a swept attachment line boundary layer in compressible flow, extending earlier work by Theofilis, Fedorov, Obrist and Dallmann (2003). Using the BiGlobal EVP code, Theofilis was able to verify (and modify) analytical predictions of Fedorov (Moscow Institute of Physics and Technology, RU), while Collis (Sandia Labs, USA) is preparing DNS work on the infinite swept cylinder geometry, in order to compare with results of the previous two approaches. Results were presented in the invitation-only IUTAM Symposium *"One Hundred Years Boundary Layer Research",* Göttingen, Germany, Aug. 12-14, 2004 and a first publication on this topic (of ongoing research) has been generated and will appear in the proceedings of this prestigious Symposium.

6. New developments for open and full-bay models

6.1. Spectral multi-domain algorithms

One of the main conclusions of the scientific exchanges with the Caltech group has been the identification of the need for a novel multi-domain discretization of the partial-differential-equation-based BiGlobal eigenvalue problem, a topic at the heart of the project owing to the geometry of two- and three-dimensional cavities. The need to work on this subject matter may be well inferred from the results of Figures 14, 16, 17 and 18, where it is clear that the structures unraveled by the single-domain BiGlobal EVP solver and confirmed by the linearized Navier-Stokes approach extend into the flow domain outside the cavity. Developments were thus taken up by the *nu modelling* team in order to devise a new multi-domain compressible BiGlobal EVP solver. Given that the group of Colonius has focused on high-order finite-difference schemes it was decided by Theofilis to work with an alternative numerical methodology, namely spectral collocation. In this manner, value was added to the project in terms of the ability to cross-validate results using independent numerical methodologies.

Initial work on the subject of multi-domain discretization of partial differential equations focused on four aspects: solution of linear systems and eigenvalue problems in one and two spatial dimensions, respectively. Model elliptic problems, such as a one-dimensional linear equation having as solution the quadratic function and the two-dimensional linear equation

$$\Delta u = 10 \cdot \sin(8 \cdot x \cdot (y-1)) \qquad in\ \Omega = [-1,1]x[-1,1]$$
$$u = 0. \qquad in\ \partial\Omega$$

were solved. Results of spectral multi-domain solutions of the 1D linear equation, defined on $x \in [-2, 2]$, and of the 2D problem defined above are shown in Figure 19. Excellent performance of the multi-domain scheme may be seen in the solution of both the 1- and the 2-D problem.

Subsequent work built upon the success of the previous efforts in solving elliptic partial differential equations and extended this technology to tackling eigenvalue problems. Two classes of EVPs were solved, the Orr-Sommerfeld equation, which is the 1-D limit of the incompressible BiGlobal EVP, as well as partial-differential-(Poisson-)-equation-based scalar two-dimensional eigenvalue problems. Both are essential stepping stones in order to be able to solve the BiGlobal EVP in the open cavity. A key validation step included well-studied limiting cases based on the equations of fluid flow motion, the best known of which is the Orr-Sommerfeld equation. The latter equation has been solved using two one-dimensional domains connected by imposing C^1 continuity at y=0, and resolved using 32 collocation points per subdomain. The parameters shown by Canuto, Hussaini, Quarteroni and Zang (1987), Re=7500, α=1, have been chosen for comparison. Excellent agreement between the corresponding eigenvalue and the published results has been obtained, while the dominant real part of the eigenfunction is presented in graphical form in Figure 20.

The excellent agreement between the literature results and those delivered by our novel spectral multi-domain technique suggests that the latter is well-suited to study the open cavity flow BiGlobal instability problem. However, prior to addressing the Navier-Stokes based EVP, the last validations performed have concerned eigenvalue problems involving the Poisson equation, which is an essential part of the linearized operator describing BiGlobal instability analysis (Theofilis 2003).

Figure 19: Upper: a quadratic one-dimensional function obtained on four domains comprising 8, 8, 16 and 32 collocation

points. Lower: numerical solution of a two-dimensional elliptic problem on a single 2D domain comprising 25x25 points and on four 2D domains, each comprising 12x12 points.

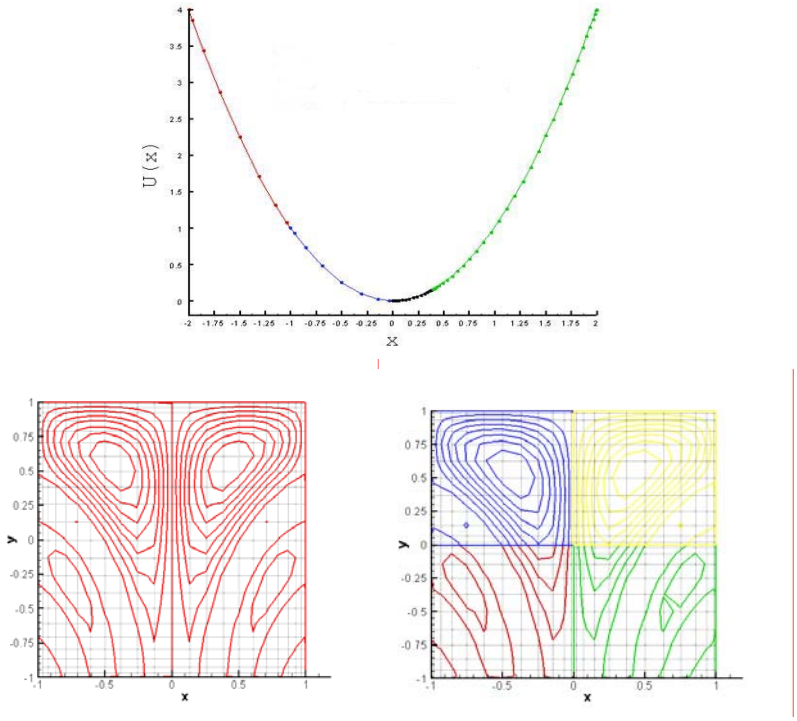

Figure 20: Multi-domain solution of the Orr-Sommerfeld eigenvalue problem in plane channel flow. Shown is the real part of the amplitude function of the wall-normal perturbation at Re=7500, α=1; domains connected at y=0.

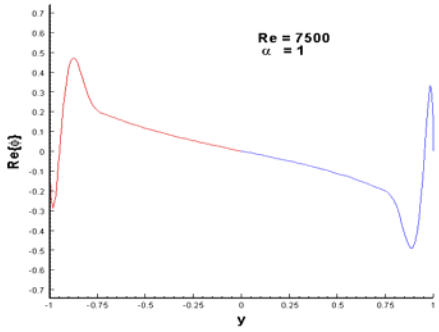

The model EVP based on the Poisson equation that has been addressed has been suggested by Trefethen (2000):

$$-\Delta u + f(x,y)u = \lambda u \qquad en\ \Omega = (-1,1)$$
$$u = 0 \qquad en\ \partial\Omega$$

Taking $f = 0$ the eigenfunctions may be obtained analytically by separation of variables and have the form:

$$\sin(k_x(x+1))\sin(k_y(y+1))$$

where k_x and k_y are integer multiples of $\frac{\pi}{2}$. Consequently the eigenvalues are also analytically known:

$$\frac{\pi^2}{4}(i^2 + j^2), \qquad i, j = 1, 2, 3, ...$$

making this problem a good candidate to study the properties of a novel numerical scheme. Discretization of the model EVP using spectral collocation and the multidomain technique results in the EVP of the form

$$(LHS)u = \lambda (RHS)u$$

where λ is the sought eigenvalue, $LHS = (-\Delta + f(x,y))$ and, here, RHS is the identity matrix.

First, single-domain computations delivered the following results for the four most significant eigenvalues:

Table 7: Single-domain solution of the model two-dimensional EVP $-\Delta u + f(x,y)\, u = \lambda u$ for $f=0$.

	Analytical result	Present numerical solution
1	$2\cdot\pi^2/4 = 4.93480220054467$	4.934802200544
2	$5\cdot\pi^2/4 = 12.33700550136169$	12.337005501361
3	$5\cdot\pi^2/4 = 12.33700550136169$	12.337005501363
4	$8\cdot\pi^2/4 = 19.739208802178717$	19.739208802178

Taking $f(x,y) = \exp(20(y-x-1))$ only single-domain numerical solutions of this problem are known, one of which is presented by Trefethen (2000) in terms of the eigenvalues:

Table 8: Single-domain solution of the model two-dimensional EVP $-\Delta u + f(x,y)\, u = \lambda u$ for $f = \exp[20(y-x-1)]$.

	Trefethen (2000)	Present numerical solution
1	$2.116423652153\cdot\pi^2/4$	5.221491363672
2	$5.023585398303\cdot\pi^2/4$	12.394945792404
3	$5.548908101834\cdot\pi^2/4$	13.689074320561
4	$8.642804449790\cdot\pi^2/4$	21.323357787175

The corresponding eigenfunctions are shown in Figure 21.

Figure 21: The first four eigenmodes of the 2-D Poisson EVP corresponding to *f(x,y)=exp(y-x-1)*, solved using single-domain spectral collocation

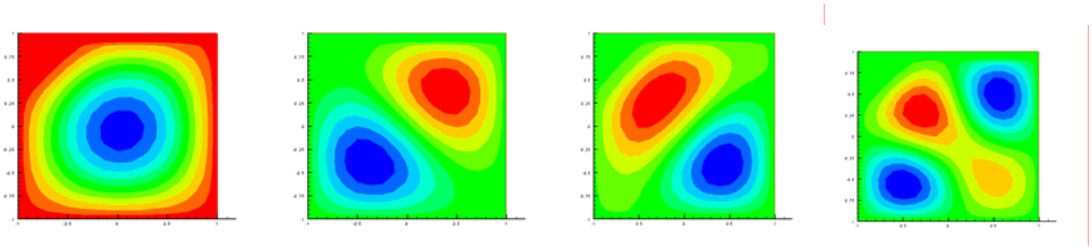

The same EVP is then solved using the novel spectral multi-domain technique. Two and four subdomains have been considered, each being resolved by 21^2 collocation nodes. C^1 continuity of the solution across subdomain boundaries has been imposed. Results have been obtained for two cases of the forcing function $f(x, y)$, one corresponding to analytically- and the other to only-numerically-known results; these are presented in the following tables:

Table 9: Multi-domain solution of the model two-dimensional EVP $-\Delta u + f(x,y)\, u = \lambda u$ for $f = 0$

	Analytical value	Present solution – 2 domains	Present solution – 4 domains
1	4.93480220054467	4.934802200541	4.934802200538
2	12.33700550136169	12.337005501359	12.337005501895
3	12.33700550136169	12.337005501362	12.337005501900
4	19.73920880217871	19.739208802180	19.739208803263

Table 10: Multi-domain solution of the model two-dimensional EVP $-\Delta u + f(x,y)\, u = \lambda u$ for $f = \exp[\,20\,(y-x-1)\,]$.

	Trefethen (2000) single-domain	Present solution single-domain	Present solution – 2 domains	Present solution – 4 domains
1	$2.116423652153 \cdot \pi^2/4$	5.221491363672	5.221445153111	5.221849381051
2	$5.023585398303 \cdot \pi^2/4$	12.394945792404	12.394904449197	12.395128398195
3	$5.548908101834 \cdot \pi^2/4$	13.689074320561	13.688868122805	13.690499067793
4	$8.642804449790 \cdot \pi^2/4$	21.323357787175	21.323199763726	21.324400372510

while the corresponding eigenfunctions, obtained in two domains joined at x=0, are shown in Figure 22.

Figure 22: The first four eigenmodes of the 2-D Poisson EVP solved using *f(x,y)=exp(y-x-1)*, solved using the novel multi-domain spectral collocation technique.

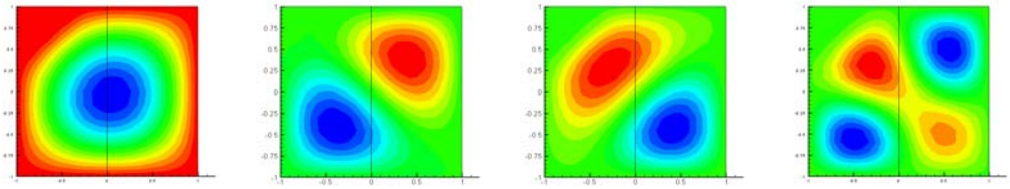

The excellent agreement between analytical and numerical results has built additional confidence in the newly-developed methods in order to apply them to the BiGlobal eigenvalue problem. For the sake of simplicity of the presentation of the methodology followed, in Figure 23 flow in a square domain in the incompressible limit is considered. The square is subdivided in four subdomains, denoted by the colors red, green, dark- and light blue. The disturbance equations are written in each of the domains, as schematically shown. As a matter of fact, an essential requirement of the spectral multidomain algorithm developed, not shown in Figure 23, has been its non-conforming nature, namely its ability to discretize neighboring domains with different resolutions. This requirement was imposed on the algorithm with a view to be able to resolve subdomains away from the solid surface of the cavity by relatively coarse meshes, while selectively reserving high resolution for boundary layers and downstream corners in the cavity. This requirement added to the complexity of the overall non-conforming spectral multidomain algorithm, especially with respect to the imposition of distinct types of boundary conditions. Figure 24 provides a graphical representation of the situation encountered at the interface of non-conforming elements, while Figure 25 extends and completes Figure 23, in that the means of imposition of the two types of Dirichlet or Neumann boundary conditions, as well as that of the compatibility conditions at the interface are shown.

Figure 23: Extension of the spectral multi-domain technique to the BiGlobal EVP. Conforming-domain discretization.

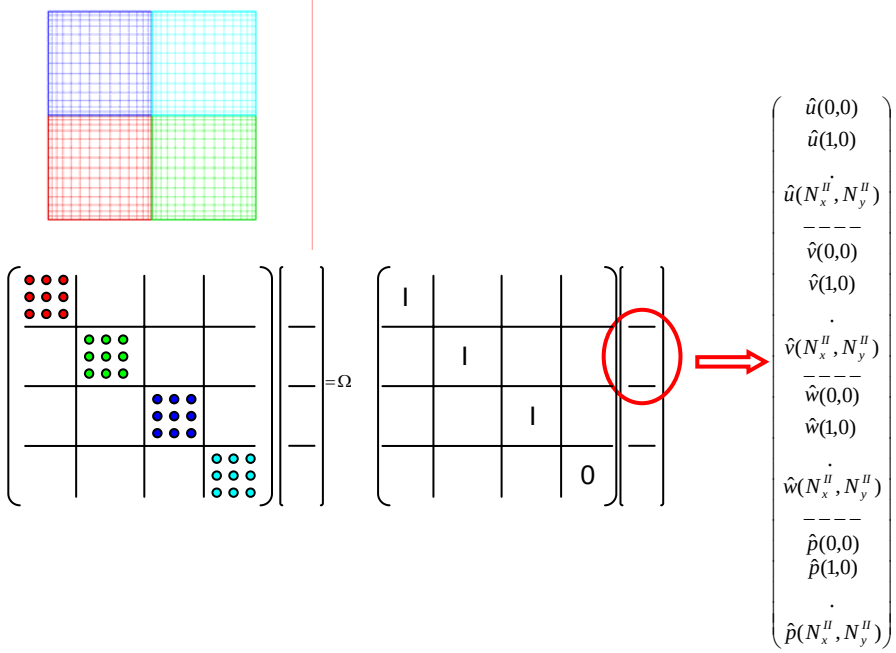

Figure 24: Typical interface of two subdomains in the non-conforming spectral multidomain technique developed.

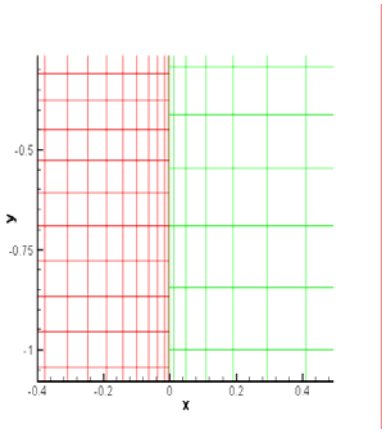

Figure 25: Details of the imposition of Dirichlet- and Neumann-type of boundary conditions and of compatibility conditions at the interface of neighboring subdomains in the solution of the BiGlobal EVP by the non-conforming spectral multidomain technique.

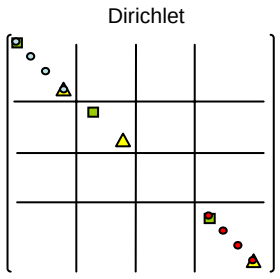

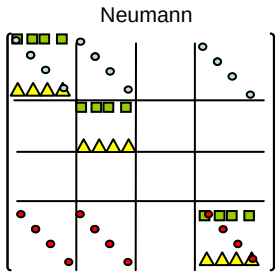

B.C. x max
B.C. x min
B.C. y max
B.C. y min

$$\hat{u}^1(N_x,y_i)-(I_2^1\hat{u}^2(0,x_0)+..+I_2^1\ \hat{u}^2(0,x_{N_x^2}))=0$$
$$\hat{v}^1(N_x,y_i)-(I_2^1\hat{v}^2(0,x_0)+..+I_2^1\ \hat{v}^2(0,x_{N_x^2}))=0$$
$$\hat{w}^1(N_x,y_i)-(I_2^1\hat{w}^2(0,x_0)+..+I_2^1\ \hat{w}^2(0,x_{N_x^2}))=0$$
$$\hat{p}^1(N_x,y_i)-(I_2^1\ \hat{p}^2(0,x_0)+..+I_2^1\ \hat{p}^2(0,x_{N_x^2}))=0$$

.

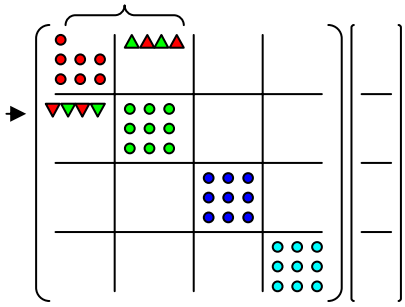

$$\hat{u}_x^1(N_x,y_i)-(I_2^1[D_x(x_0,x_0)\hat{u}^2(x_0,y_0)+..$$
$$+\ D_x(x_0,x_{N_x^2})\hat{u}^2(x_{N_x^2},y_0)]+...$$
$$+I_2^1[D_x(x_0,x_0)\hat{u}^2(x_0,y_{N_y^2})+...$$
$$+\ D_x(x_0,x_{N_x^2})\hat{u}^2(x_{N_x^2},y_{N_y^2})])=0$$

6.2. Finite-element algorithms

In view of the ultimate aim of this avenue of research, instability analysis of complex full-bay models of open cavity flows, the necessity arises to compute steady basic states around such configurations. One option would have been to extend and adapt the Caltech high-order accurate DNS code to provide such states on conformable regular (rectangular) subdomains. Instead, we opted for finite-element solutions on unstructured meshes, an approach which permits resolution of both structured rectangular domains, as well as more complex irregular geometries of cavity bays, and ultimate consideration of arbitrarily-shaped (including curved) stores. During the current validation stages, assumptions were relaxed in a systematic manner, departing from the well-understood and documented rectangular cavity configuration. The cavity geometry and unit Reynolds number have been defined, scaling lengths with the cavity depth, D. An analytic model of the (Blasius) flat plate boundary layer has been developed and imposed at the inflow boundary. In order to recover the steady basic states to be analyzed, points in the multi-parametric space (Reynolds number, thickness of the boundary layer at the cavity lip, length-over-depth of the cavity) have been identified, at which such steady states exist. Basic flows have been computed on unstructured grids, typically comprising $O(10^5)$ triangular elements, distributed in a manner that refines critical calculation areas such as the boundary layers and the cavity corners; a typical mesh at Re =1600 is shown in Figure 26.

Figure 26: Typical unstructured mesh used for the finite element solution of the basic flow problem, here at Re=1600.

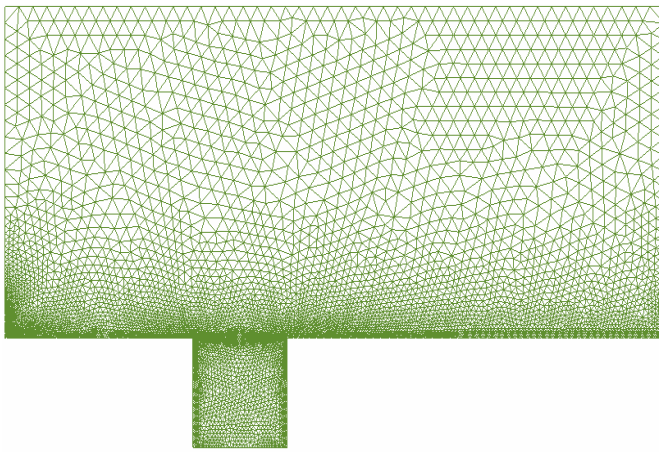

Regarding the spectral multi-domain BiGlobal eigenvalue problem solution algoritm subsequently used, the basic flow obtained by the finite-element method was interpolated from a subset of the unstructured mesh on each subdomain of the spectral multi-domain grid, in a manner that will be described shortly. In order to resolve well areas where the sought eigenvectors are expected to attain their maxima, two strategies have been investigated. First, the geometric features of the open cavity were taken into account, dividing space into four major rectangular subdomains, one being the cavity itself, and the other three being defined upstream-, above- and downstream of the cavity. Each of the four subdomains was stored on a different processor of the computing cluster and was discretized independently, adding points to the appropriate subdomain (typically that inside the cavity) until convergence was achieved. This strategy was soon abandoned since the resolution requirements in specific subdomains are such that the available memory of the computing node at which those subdomains resided quickly became inadequate, while the availability of the cluster computing nodes was not fully exploited.

A second strategy was then followed, in which the same four subdomains have been further subdivided and the resulting subdomains have been distributed, one per processor. Since the resulting subdomains are substantially smaller in size in the latter strategy, it is straightforward to refine only those parts of space where the eigenmode resides; in turn full advantage is taken of the existence of several processors of the computing cluster. It has to be noted that the latter approach relies precisely on the availability of the computing cluster described in Section IV.1 and further justifies the initially projected need for investment on hardware appropriate to support the numerical work of this Grant. Parallelism has been achieved through performing the residual matrix operations using iterative algorithms, as implemented in standard (distributed) libraries.

The overall computational strategy for the recovery of BiGlobal instability results using the non-conforming spectral multidomain algorithm is shown in Figure 27. A key difference with the previously used QZ and IRAM approaches for the computation of the eigenspectrum is that in the present distributed computing strategy the matrix discretizing the eigenvalue problem is never formed explicitly, although the (parallel) Arnoldi algorithm is still used. By contrast to the previously used approach, the matrix is formed using the compressed column format (CCF) scheme, as opposed to the dense matrix storage used in the BiGlobal solutions presented in Sections IV. 4 – 5. In the present CCF formulation only the non-zero entries of the matrix are kept in memory and are then processed by the iterative solution software.

Figure 27: Overall solution algorithm for the BiGlobal EVP resulting from non-conforming spectral multidomain spatial decomposition.

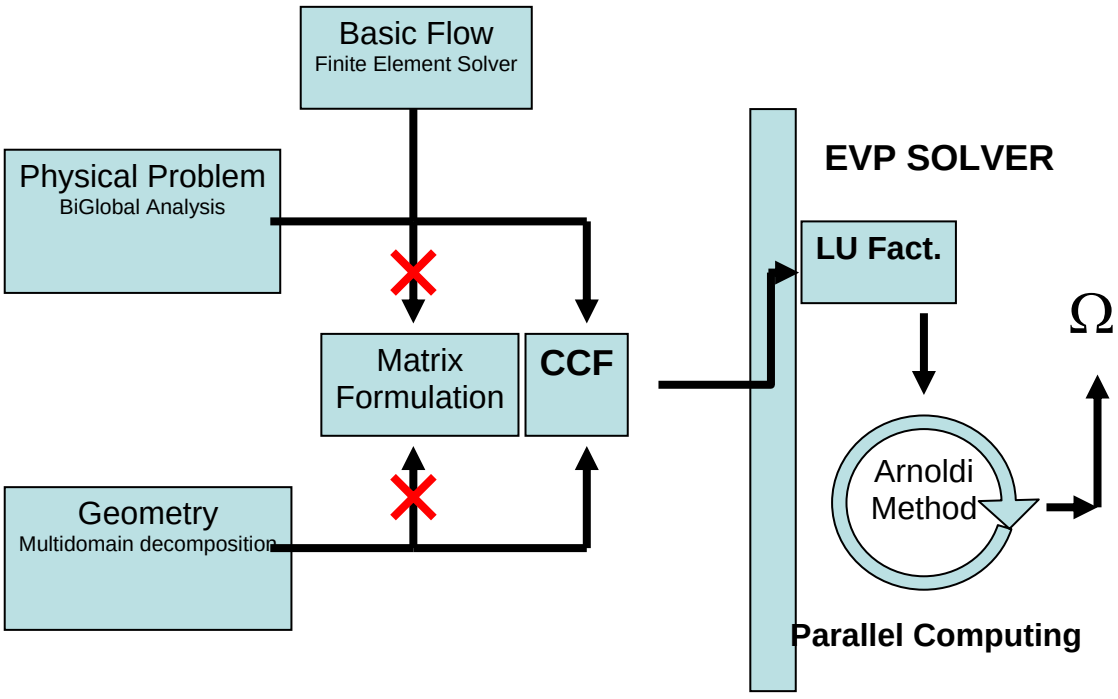

With all the algorithms in place and validated, efforts were then directed toward the solution of the incompressible BiGlobal EVP in a simple geometry, previously analyzed in the EOARD-funded work of Theofilis et al. (2004), namely stable flow in the lid-driven cavity at Re =200, β=1. Both the single-domain case and two multi-domain cases were solved with the same newly developed code. The minimum nontrivial discretization involves partition of the square into two sub-domains, denoted "red" and "green", each of which is discretized using the same number of collocation points as in the single-domain case, 32 in each spatial direction. Excellent quantitative agreement has been obtained between the literature value and those obtained using the multi-domain technique, maximum differences in the eigenvalues being confined below the fourth significant place. The amplitude functions of the leading member of the eigenspectrum obtained through the three approaches are shown in Figure 28. **These results demonstrate that the first-ever solution of the incompressible BiGlobal eigenvalue problem in multiple domains has been obtained in the framework of the present Grant.**

Figure 28: The spatial structure of the streamwise- and transverse- disturbance velocity and disturbance pressure amplitude functions pertaining to the leading eigenvector of the lid-driven cavity flow at Re=200, β=1, as delivered by single-domain and two alternative multi-domain solutions of the BiGlobal EVP (Theofilis, Duck & Owen *JFM* **505** 2004)

Single-domain BiGlobal analysis (Theofilis, Duck & Owen JFM **505**, 249-286, 2004)	Multi-domain BiGlobal analysis 2 domains connected at x=0.5 (present analysis)	Multi-domain BiGlobal analysis 2 domains connected at y=0.5 (present analysis)
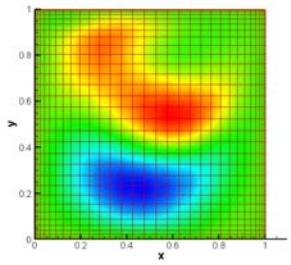	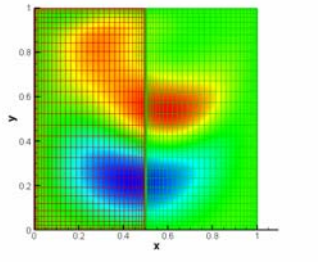	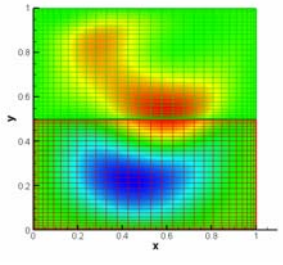
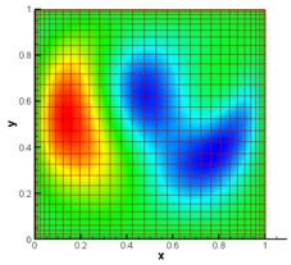	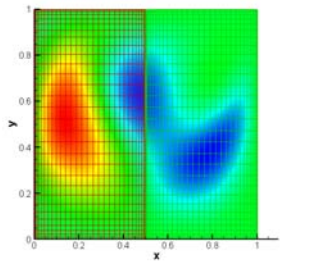	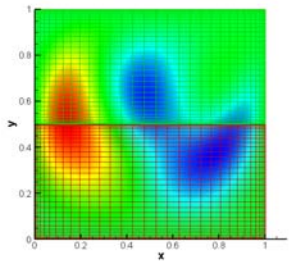
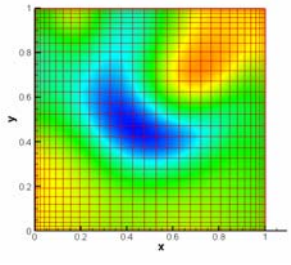	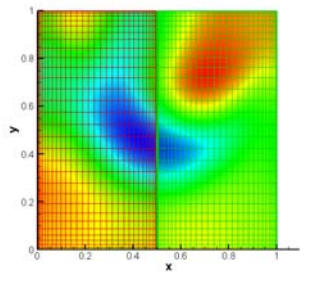	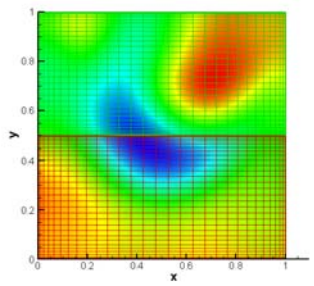

Next, attention has been paid to the open cavity configuration. A steady laminar basic flow was obtained by the finite-element algorithm at Re=1600, as shown in Figure 29. The marked area of the flowfield in the neighborhood of the cavity was extracted and interpolated on a non-conforming spectral multidomain grid, as also shown in this figure. Grid independence tests ensured the quality of the interpolations and provided the variable coefficients for the subsequent numerical solution of the three-dimensional BiGlobal eigenvalue problem.

Figure 29: Left column shows typical basic flows obtained by the finite-element method. The area within the dotted box is extracted and analyzed. Right column: close-up of the interpolated basic flow velocity components, with the non-conforming spectral multi-domain discretization clearly visible.

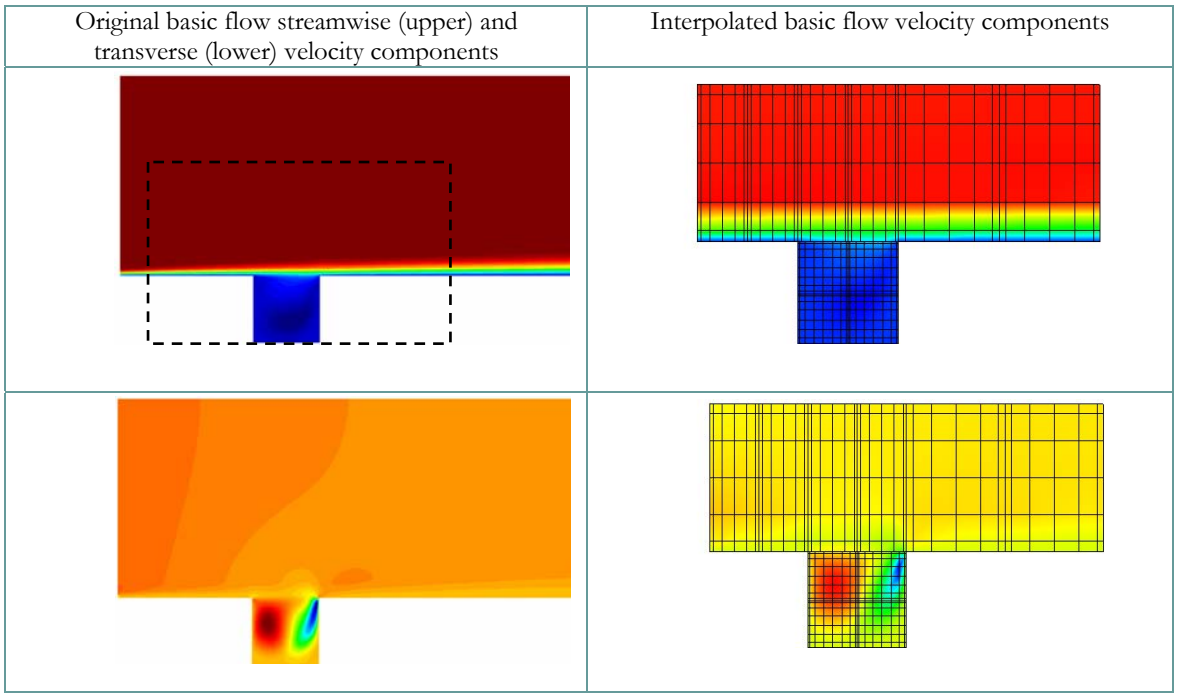

The first two stationary modes, obtained at Re =1600, and spanwise wavenumber β=1, are shown in Figure 30 in terms of their respective three components of the disturbance velocity amplitude functions. Here 16 subdomains have been used, those outside the cavity having been resolved using 12 spectral collocation points in each spatial direction, while each of the four subdomains inside the cavity has been resolved using 24 spectral collocation points per direction. It is interesting to notice that at these parameters, instability activity is confined within the cavity, where all amplitude functions attain their respective maxima, while the disturbance flowfield outside the cavity remains benign. These conditions are reminiscent of the instability mechanisms unraveled by the residuals algorithm and presented in Figure 8, both situations being apparently related with the wake mode instability. In such situations, a-posteriori justification for the (computationally less intensive) approach of Theofilis and Colonius (2004) may be provided. However, other types of disturbances extending beyond the cavity may well be associated with this configuration, which can only be resolved by the present general approach. We refrain from further (speculative) elaboration on these point here but note that linear amplification of such modes will lead the steady laminar basic flow shown in figure 29 into unsteadiness (on account of growth of the eigenmode and/or its nonzero frequency) and three-dimensionality (on account of $\beta \neq 0$) and it is worth investigating whether turbulence or nonlinear limit cycles is the result of such amplification. These questions, as well as further physical interpretation of these results, are the topics of a publication in preparation.

Figure 30: The first three-dimensional solutions of the direct BiGlobal EVP in an open cavity configuration at Re=1600, β=1 , incorporating the entire cavity domain in the solution. Shown are the first two stationary modes in the cavity.

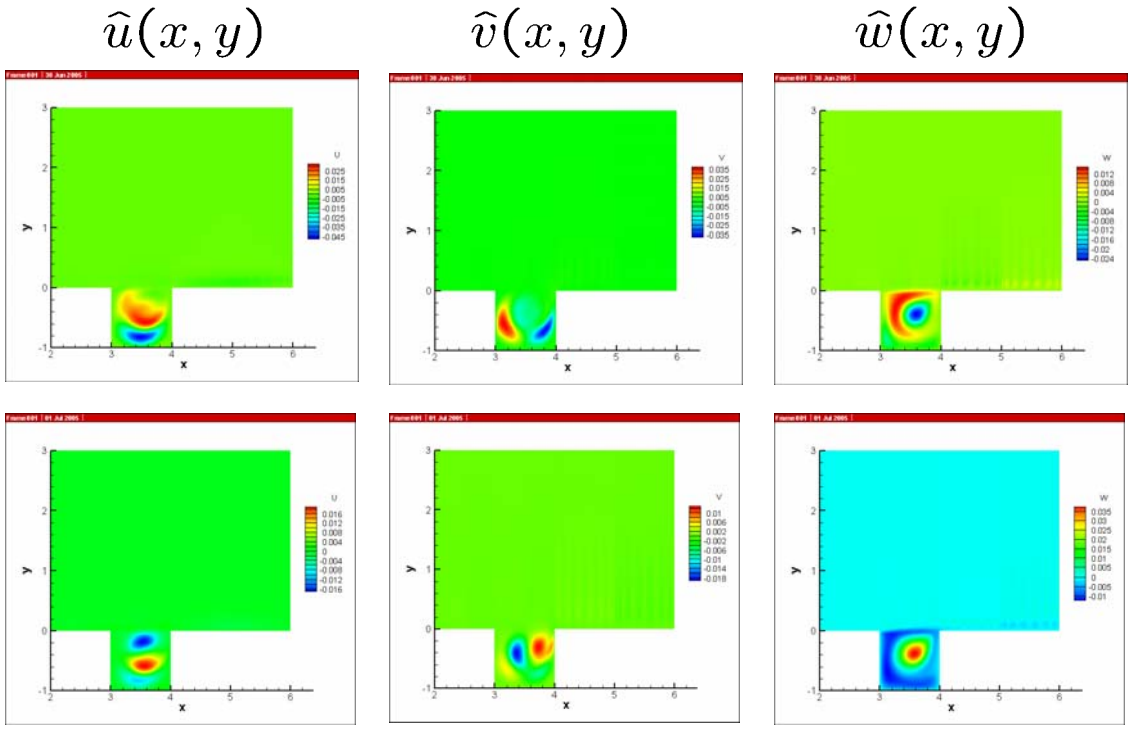

However, worthy of mention in these results, and others obtained but not shown here in the same parameter range, is **the qualitative analogy of the spatial structure of the leading stationary eigenmodes of the open and the lid-driven cavity flow** (Theofilis 2000). For comparison, the spanwise disturbance velocity component of the lid-driven cavity flow is shown in Figure 31. It is interesting that structures corresponding to essentially nonparallel flows are present in both cavity configurations. None of them appears to be related with the well-studied KH shear-layer instability, which is not surprising in the lid-driven but is remarkable in the open-cavity configuration.

Figure 31: The spanwise disturbance velocity component of the lid-driven cavity flow (Theofilis Duck & Owen *JFM* **505** 2004).

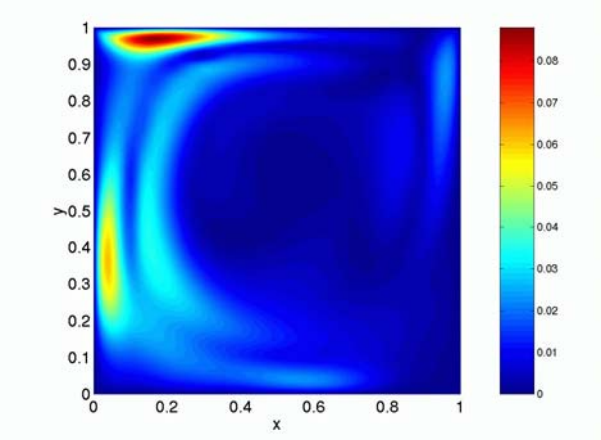

It is a straightforward matter to analyze different open cavity configurations using the developed methodology. From a physical point of view it is necessary to lower the Reynolds number below that used in the square cavity analysis in order to obtain a steady state, a situation which is consistent with the linear BiGlobal instability scenario in the lid-driven cavity (Theofilis *et al.* 2004). In Figure 32 results are presented of an analysis of L / D = 2 flow at Re = 400 and β = 1. The leading travelling and stationary eigenmodes are shown in terms of the magnitude of the amplitude functions of the three disturbance velocity components. Interestingly, the (spanwise-) travelling disturbance is also situated inside the cavity, while the stationary mode extends in the shear-layer region. The three-dimensional (out-of-plane) disturbance velocity component of both modes shows strong peaks in the downstream corner of the cavity. Systematic studies of the multidimensional parameter space are currently underway; however, the following discussion focuses on a different aspect of cavity instability, using the L/D=2 results of Figure 32 as reference.

Figure 32: Amplitude functions of the leading traveling and stationary mode in an aspect ratio 2 open cavity at Re=400, spanwise wavenumber, β=1.

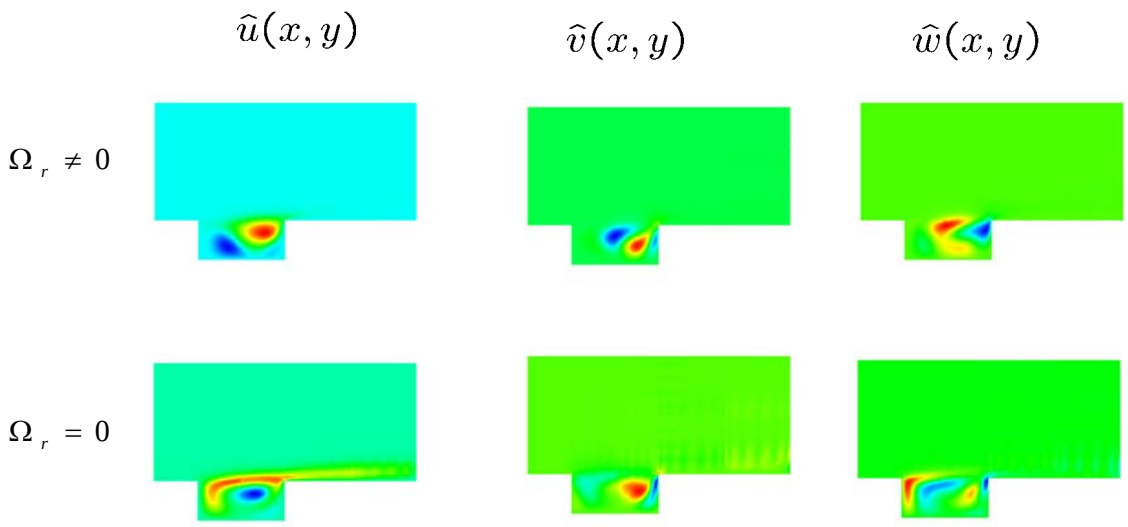

6.3. On open- v. full-bay cavity instability

The key question which led to the development of the non-conforming spectral multidomain algorithm has been the investigation of the potential influence that stores inside an open cavity may have on the instability characteristics of the cavity. Answering this question has been facilitated by the newly developed multi-domain algorithm, which permits defining and analyzing efficiently any regular decomposable domain, concretely in the case of the open cavity, any rectangular decomposable domain. The simplest model store configuration possible, namely a rectangular object placed inside an open cavity, was considered as a demonstrator and has been analyzed with respect to its BiGlobal instability. The basic states corresponding to the aforementioned model problem are shown in Figure 33. While the streamwise velocity component is hardly affected by the presence of the object, strong modifications of the transverse basic flow velocity component may be seen. The main result of the subsequent instability analysis is that this O(1) modification of the basic state results in significant departure of the instability characteristics of a cavity containing objects from those of the reasonably well-understood (empty) open cavity configuration. A demonstration of this fact may be seen in Figure 34, in terms of the leading stationary eigenmode of the configurations presented in Figure 32, at the same flow parameters.

Figuqqre 33: Upper row: Streamwise- (left) and transverse (right) basic flow velocity components of incompressible flow over an aspect ratio 2 (empty) open cavity at Re=400. Lower row: Same result with a model store placed inside the cavity.

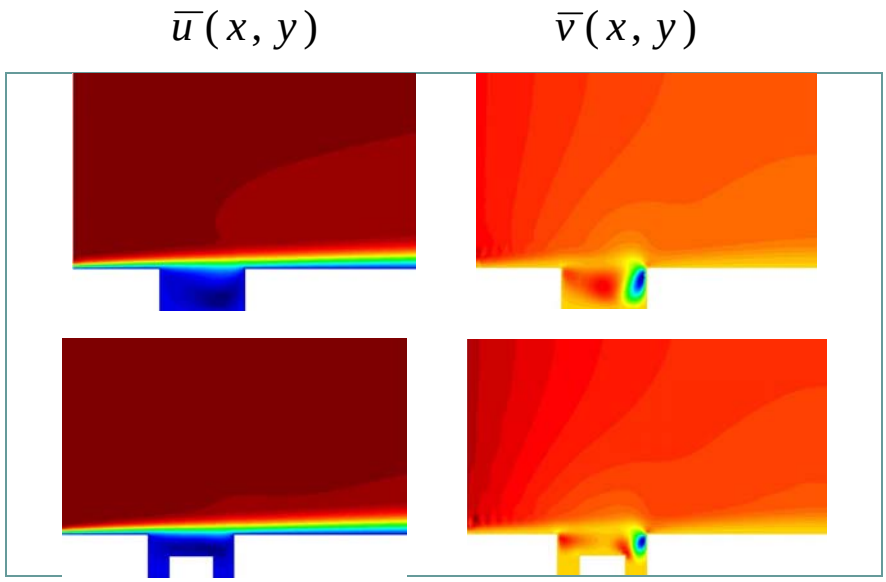

Figure 34: Upper row: Streamwise- (left), transverse (middle) and spanwise (right) disturbance flow velocity components of the open cavity basic flow shown in Figure 1, at Re=400, spanwise wavenumber, β=1. Lower row: Corresponding result with an object placed inside the cavity.

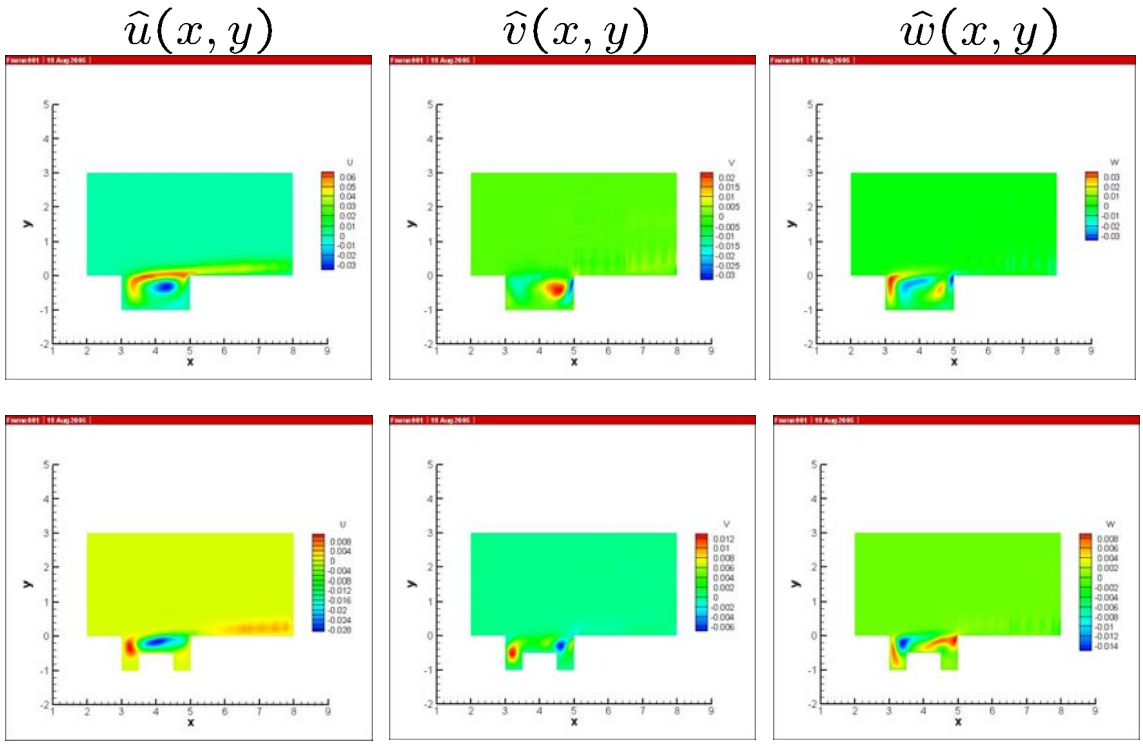

The final class of problem solved involved full utilization of the potential of the multidomain algorithm in terms of a model store of higher complexity compared with that shown in Figures 33 and 34. This so-called "T-store" configuration, alongside the non-conforming multidomain grid used to analyzed it, is shown in Figure 35. Note that 29 sub-domains have been used in order to resolve the geometry properly, devoting a large number of Chebyshev Gauss-Lobatto nodes in the neighborhood of large gradients and progressively relaxing the resolution requirements away from the boundary layers and the cavity/store walls. The flexibility of the algorithm developed is borne out by the non-conforming nature of the sub-domains. Its efficiency may be appreciated in noting that each BiGlobal eigenvalue computation of this configuration at one set of (Re,β) parameters requires approximately 800 seconds of (parallel) computation. For the analysis the same parameters as those used in the results presented in Figures 32 and 34 have been used.

Figure 35: Domain decomposition and 2D-Chebyshev Gauss-Lobatto grids utilized for the BiGlobal instability analysis of the T-store configuration

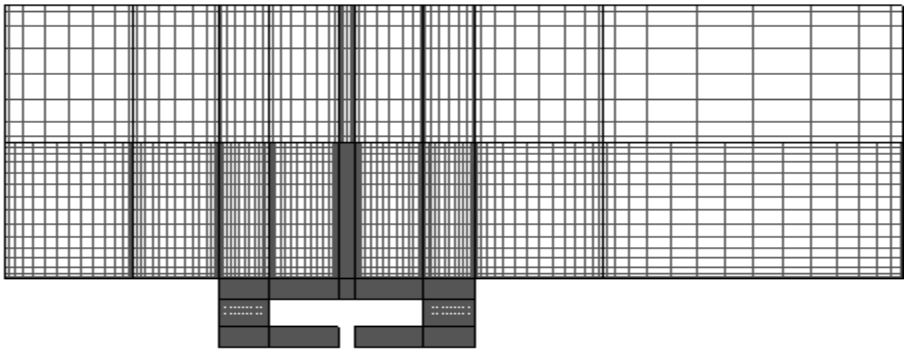

Figure 36: The leading BiGlobal eigenmodes of the T-store configuration at the parameters shown in Figure 34.

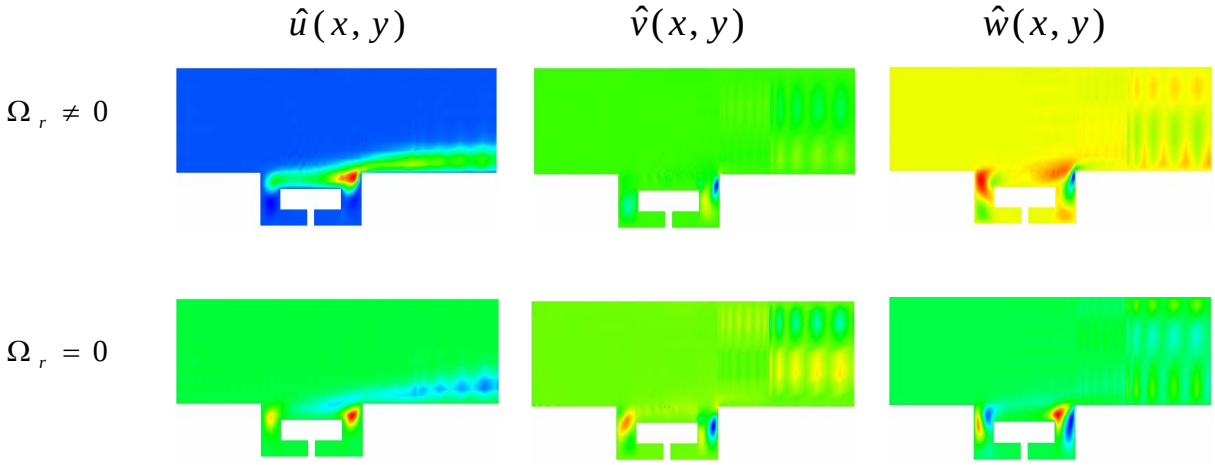

Again, the particular characteristics of the T-store basic flow (not shown here) have been found to have a profound influence on the corresponding instability characteristics. The leading two eigenmodes of the open cavity in the presence of the T-store model are shown in Figure 36, in terms of the amplitude functions of the disturbance velocity components. Besides the fact that frequencies of traveling modes are O(1) apart compared to those found in the analyses summarized in Figure 32 and 34, it is noted that the introduction of additional corners in the geometry results in additional peaks appearing in the amplitude functions of the components of the stationary eigenmodes, pointing to regions that potentially would need to be controlled in the flow.

Summarizing this part of the research, it becomes clear that instability characteristics such as amplification rates and frequencies of the leading eigenmodes in the three open cavity configurations addressed (empty, rectangular-object, T-store) are **distinct**. While from a theoretical point of view either of the three (or indeed any other related) models could be selected and analyzed in detail, our work has demonstrated for the first time that, if answers relevant to Air Force applications are sought, one should focus on a model of an open-cavity-plus-stores as close as possible to the actual application. In this respect, the algorithms developed during the course of the present Grant provide a flexible and efficient tool to support such efforts.

V. SUMMARY AND FUTURE DIRECTIONS

The novel BiGlobal instability analysis approach was applied for the first time to incompressible and compressible flows over open cavities. Two distinct methodologies have been developed, an extension of the residuals algorithm, previously demonstrated in the lid-driven cavity problem, and direct solutions of the BiGlobal EVP. The latter methodology itself has followed two different paths, single-domain computations of the eigenspectrum disturbances inside the cavity in isolation from the flowfield outside the cavity, and multidomain computations of the eigenspectrum corresponding to the entire two-dimensional cavity flowfield. Finally, the multidomain algorithm itself was applied to both (empty) open and full-bay model cavity configurations.

Consistently, the results obtained by all novel approaches presented herein have opened new research avenues. The residuals algorithm offered a new unified perspective of known hydrodynamic and aeroacoustic instabilities, in addition to providing access to previously unknown (or not recognized as such) linear disturbances of this flow; results of the systematic application of the residuals algorithm will be presented by the Caltech team. The direct solutions of the BiGlobal eigenvalue problem have been the first-ever successful solutions of the problem of linear instability in the open cavity, without the need to resort to the strong assumption of parallel or near-parallel flow, as invariably done in previous research. As such, structures inaccessible to classic linear analysis of the Kelvin-Helmholtz / Tollmien-Schlichting / Parabolized Stability Equations class have been unraveled by the BiGlobal approach. In view of the BiGlobal instability results obtained in the framework of the present effort, it is clear that future instability analyses of cavity flows, aiming at producing a full picture of linear mechanisms at specific parameter ranges, must consider the problem of small-amplitude disturbance excitation from the broader, BiGlobal, perspective. In turn, efforts aiming at providing theoretically-founded approaches to flow control by control of flow instability must answer the question of how to control unstable traveling and stationary BiGlobal eigenmodes, in addition to controlling well-understood feedback-loop mechanisms. Finally, if the relevance of cavity research to the warfighter is to be increased, the present research has shown that a close model of the cavity geometry, including modeling the stores, is not only necessary but also feasible, thanks to the numerical methodologies developed herein.

Regarding future directions, in the opinion of the author, two areas are considered as potentially extremely fruitful. First, secondary BiGlobal theory, extending the tools presented herein to include Floquet theory, could be used in order to analyze time-periodic cavity flows at Reynolds numbers above the relatively low ones at which steady states exist. Second, the BiGlobal approach could be combined with Reynolds-averaged Navier-Stokes (RaNS) predictions, in order to analyze (BiGlobal) instability of the turbulent flow at flight Reynolds and Mach numbers. Both suggested avenues are feasible: secondary BiGlobal theory has recently been demonstrated by the author in the Low Pressure Turbine instability problem (see Final Report of Grant F49620-03-1-0295 on the subject). On the other hand, Crouch (2005) has arrived at excellent predictions of the wing-buffeting problem, analyzing for the first time a RaNS solution by a compressible BiGlobal instability approach. Both research avenues could directly incorporate the newly-developed spectral multidomain techniques in order to analyze instability of full-bay configurations at realistic flight conditions and thus provide theoretically-founded answers to issues directly relevant to the warfighter.

REFERENCES

Alvarez J., Kerschen E., and Tumin A.. A theoretical model for cavity acoustic resonances in subsonic flow. AIAA Paper 2004-2845, 2004.

Barkley D., Gomes M.G.M., and Henderson R.D. Three dimensional instability in flow over a backward-facing step. J. Fluid Mech., 473:167–190, 2002.

Benson J. D. and Aidun C. K.. Transition to unsteady nonperiodic state in a through-flow lid-driven cavity. Phys. Fluids A, 4:2316–2319, 1992.

Blumen, W. Shear layer instability of an inviscid compressible fluid. J. Fluid Mech. 40(4):769-781, 1970.

Cain, A., Rubio A. D., Bortz, D. M., Banks, H. T. and Smith R. C.. Optimizing control of open bay acoustics. AIAA Paper 2000-1928, 2000.

Canuto C., Hussaini, M. Y., Quarteroni, A. and Zang, T. A. Spectral methods in fluid dynamics, Springer, 1987

Crouch, J. D. On the onset of buffet on a NACA-0012 wing at an angle of attack. 3rd Global Flow Instability and Control symposium, Crete, Greece, Sept. 25 – 28, 2005.

Forestier, N. Jacquin, L. and Geffroy P.. The mixing layer over a deep cavity at high- subsonic speed. J. Fluid Mech., 475:101–145, 2003.

Fuglsang D.F. and Cain A.B.. Evaluation of shear layer cavity resonance mechanisms by numerical simulation. AIAA Paper 92-0555, 1992.

Gharib, M. and Roshko, A. The effect of flow oscillations on cavity drag. J. Fluid Mech., 177:501–530, 1987.

Gloerfelt, X. Bogey, C. Bailly C., and Juve D.. Aerodynamic noise induced by laminar and turbulent boundary layers over rectangular cavities. AIAA Paper 2002-2476, 2002.

Hammond D. A. and Redekopp L. G.. Local and global instability properties of separation bubbles. Eur. J. Mech. B/Fluids, 17:145–164, 1998.

Jackson A. P., Hillier R., and Soltani S.. Experimental and computational study of laminar cavity flows at hypersonic speeds. J. Fluid Mech., 427:329–358, 2001.

Kriesels P. C., Peters M. C. A. M., Hirshberg A., Wijnands, A. P. J. Iafrati A., Riccardi G., Piva R., and Bruggeman. J. C. High aplitude vortex-induced pulsations in a gas transport system. Journal of Sound and Vibration, 184(2):343–368, 1995.

Macaraeg, M.G. Streett, C.L. and Hussaini. M.Y. A spectral collocation solution to the compressible stability eigenvalue problem. NASA Technical Publication 1988-2858, 1988.

Mack. L. M. Boundary layer linear stability theory. In AGARD–R–709 Special course on stability and transition of laminar flow, pages 3.1–3.81, 1984.

Powell, A. On the edgetone. J. Acous. Soc. Am., 33:395, 1961

Rossiter, J. E. Wind-tunnel experiments on the flow over rectangular cavities at subsonic and transonic speeds. Aeronautical Research Council Reports and Memoranda, No. 3438, October 1964.

Rowley, C. Colonius, T. and Basu. A. On self-sustained oscillations in two-dimensional compressible flow over rectangular cavities. J. Fluid Mech., 455:315–346, 2002.

Schmid, P. J and Henningson, D. S. Stability and transition in shear flows. Springer, 2001.

Shieh C. M. and Morris P. J. Parallel computational aeroacoustic simulation of turbulent subsonic cavity flow. AIAA Paper 2000-1914, 2000.

Shieh C. M. and Morris. P. J. Comparison of two- and three-dimensional turbulent cavity flows. AIAA Paper 2001-0511, 2001.

Simens, M., González, L., Theofilis, V. and Gómez-Blanco, R. On fundamental instability mechanisms of nominally 2-D separation bubbles. IUTAM Laminar-Turbulent Symposium VI, Bangalore, India, Dec. 13-17, 2004. (R. Narasimha and R. Govindarajan eds.) Springer 2005.

Stüer, H., Gyr, A. and Kinzelbach, W. Laminar–turbulent transition of a separatin flow on a forward facing step. In W. Saric and H. Fasel, editors, Proc. of the IUTAM Laminar-Turbulent Symposium V, pages 541–546, Sedona, AZ, USA, 2000.

Tatsumi, T. and Yoshimura, T. Stability of the laminar flow in a rectangular duct. J. Fluid Mech., 212:437–449, 1990.

Theofilis, V. Globally-unstable flows in open cavities. 12 pp. AIAA Paper 2000-1965, 2000.

Theofilis, V. Advances in global linear instability of nonparallel and three-dimensional flows. Prog. Aero. Sciences, 39 (4):249–315, 2003.

Theofilis, V. and Colonius, T. An algorithm for the recovery of 2- and 3-d biglobal instabilities of compressible flow over 2-d open cavities. AIAA Paper 2003-4143, 2003.

Theofilis, V. and Colonius, T. Three-dimensional instabilities of compressible flow over open cavities: direct solution of the BiGlobal eigenvalue problem. AIAA Paper 2004-2544.

Theofilis, V., Duck, P. W. and Owen, J. Viscous linear stability analysis of rectangular duct and cavity flows. J. Fluid Mech., 505:249–286, 2004.

Theofilis, V., Hein, S. and Dallmann U. Ch. On the origins of unsteadiness and three-dimensionality in a laminar separation bubble. Phil. Trans. Roy. Soc. London (A), 358:3229–3246, 2000.

Theofilis, V., Fedorov, A., Obrist, D., and Dallmann, U. Ch. The extended Görtler-Hämmerlin model for linear instability of three-dimensional incompressible swept attachment-line boundary layer flow. J. Fluid Mech., 487:271–313, 2003.
Trefethen L. N. Spectral elements in Matlab, SIAM, 2000.

VII. OTHER ACTIVITIES SUPPORTED BY GRANT

1. Collaborations

On account of knowledge attained in the framework of the present Grant, the following new collaborations have been started:

- Dr. S. Collis (Sandia Labs) and Dr. Alexander Fedorov (Moscow Institute of Physics and Technology) on compressible attachment-line instability.
- Dr. Emmanuel Leriche (Ecole Polytechnique Federale de Lausanne, Switzerland) on cavity flows.
- Prof. Rama Govindarajan (Jawarhalal Nehru Center for Advanced Scientific Research, Bangalore, India) on large-scale computations for the BiGlobal eigenvalue problem.
- Dr. Olaf Marxen (KTH, Stockholm, Sweden) on numerical methods for the BiGlobal eigenvalue problem and DNS.

Regular contacts are kept with all these teams.

2. Visits/Student Exchanges

Theofilis spent short visits at Caltech (of typically 1 to 2 weeks) in 2002, 2003 and 2004. Partially supported by the Grant, Theofilis visited Prof. I. Gursul (Univ of Bath, UK) and attended three invitation-only meetings, namely the IUTAM Symposium "One hundred years boundary layer research", Goettingen, Germany, Aug. 2004, the NATO RTO AVT-111 meeting, Prague, Czech Republic, Nov. 2004, and the IUTAM Laminar-turbulent transition symposium VI, Bangalore India, Dec. 2004. He plans to visit Dr. Leriche (EPFL) during two weeks in July 2006.

De Vicente spent three months in the summer of 2004 at Caltech in the group of Colonius and attended the VKI Short Lecture Series "High-order methods for fluid dynamics", Nov. 2005. He plans to visit Dr. Leriche (EPFL) during the month of July 2006.

VIII. PRESENTATIONS AND PUBLICATIONS

1. Presentations

Fully- or partially (in addition to WOS or other funds) supported by the Grant

Theofilis delivered talks ate the following meetings:

- AFOSR Contractors' and Grantees' Meetings:
  - Santa Monica, CA (2002),
  - Destin, FL (2003),
  - Denver, CO (2004),
  - Long Beach, CA (2005)
  - Atlanta, GA (2006) – planned.

- Invited talks:
  - UC San Diego, CA, visiting Prof. T. Bewley
  - U of Arizona, Tucson, AZ, visiting Prof. I. Wygnanski.
- AIAA contributions:
  - Orlando, FL (2003),
  - Portland, OR (2004)
  - San Francisco, CA (2006) – planned.

De Vicente delivered talks at the following meetings:

- Universidad Politécnica de Madrid. "Implementación de métodos numéricos en maquinas de paralelo para problemas fluidodinámicos". February 2006, Madrid, Spain.
- 3rd Symposium on Global Flow Instability and Control. "Global instability of realistic open cavity flows" September 2005 Crete, Greece.

2. Publications

Fully supported by the Grant

Theofilis, V. and Colonius, T. 2003 An algorithm for the recovery of 2- and 3-D BiGlobal instabilities of compressible flow over 2-D open cavities. AIAA Paper 2004–4143.

Theofilis, V. and Colonius, T. 2004 Three-dimensional instabilities of compressible flow over open cavities: direct solution of the BiGlobal eigenvalue problem. AIAA Paper 2004–2544.

Theofilis, V., Duck, P. W., and Owen, J. 2004 Viscous linear stability analysis of rectangular duct and cavity flows Journal of Fluid Mechanics 505:249–286.

Theofilis, V., Fedorov, A. and Collis, S. S. 2004 Leading-edge boundary layer: Prandtl's vision, recent developments and future directions. IUTAM Symposium "One Hundred Years Boundary Layer Research", Göttingen, Aug. 12-14, 2004, Springer, ISBN 1-4020-4149-7.

De Vicente, J., Valero, E., González, L. and Theofilis, V. 2006 Spectral Multi-Domain Methods for BiGlobal Instability Analysis of Complex Flows over Open Cavity Configurations. 36th AIAA Fluid Dynamics Conference and Exhibit, San Francisco, CA, June 5-8, 2006.

De Vicente, J. and Theofilis, V. 2006 Non conforming spectral multidomain methods for BiGlobal instability analysis. (in preparation).

Partially supported by the Grant

Theofilis, V., Seifert, A., Joslin, R. D., and Collis, S. S. 2004 Poster on Theoretical and Experimental Active Flow Control. AIAA Summer Meeting, Portland, OR, June 28 – July 1, 2004.

Collis, S. S., Joslin, R. D., Seifert, A. and Theofilis, V. 2004 Issues in active flow control: theory, control, simulation and experiments. Progress in Aerospace Sciences 40:237–289. (***Top25* article** in Prog. Aero. Sci.)

Theofilis, V., Fedorov, A. and Collis, S. S. Leading-edge boundary-layer: Prandtl's vision, recent developments and future directions. IUTAM Symposium "One hundred years of boundary layer research", Göttingen, Germany, Aug 13-17, 2004. Springer.

Simens, M., González, L., Theofilis, V., and Gómez-Blanco, R. 2005 On fundamental instability mechanisms of nominally 2-D separation bubbles. IUTAM Laminar-Turbulent Symposium VI, Bangalore, India, Dec. 13-17, 2004. (R. Narasimha and R. Govindarajan eds.) Springer 2005.

IX. APPENDIX

The equations governing compressible BiGlobal linear instability

The linear operators appearing in the compressible BiGlobal eigenvalue problem are defined next. Over-barred quantities denote basic flow and subscripts denote partial differentiation with respect to the variable shown. The equation of state $\gamma\ M^2\ p = \rho\ T$ has been used explicitly, while M (=Ma), Pr, and Re, respectively denote Mach, Prandtl and Reynolds numbers.

Disturbance $x-$momentum:

$$
\begin{aligned}
\mathcal{L}_{x\hat{u}} &= -\tfrac{4}{3}\tfrac{\bar{\mu}}{Re}\,\partial^2_{xx} + \Big[-\tfrac{4}{3}\tfrac{1}{Re}\left(\tfrac{d\bar{\mu}}{d\bar{T}}\right)\bar{T}_x + \bar{\rho}\,\bar{u}\Big]\,\partial_x - \tfrac{\bar{\mu}}{Re}\,\partial^2_{yy} + \Big[-\tfrac{1}{Re}\left(\tfrac{d\bar{\mu}}{d\bar{T}}\right)\bar{T}_y + \bar{\rho}\,\bar{v}\Big]\,\partial_y \\
&\quad + \tfrac{\beta^2\bar{\mu}}{Re} + 2\,\bar{\rho}\,\bar{u}_x + \bar{\rho}\,\bar{v}_y + \mathrm{i}\,\beta\,\bar{\rho}\,\bar{w} + \bar{u}\,\bar{\rho}_x + \bar{v}\,\bar{\rho}_y \\
\mathcal{L}_{x\hat{v}} &= -\tfrac{1}{3}\tfrac{\bar{\mu}}{Re}\,\partial^2_{xy} - \tfrac{1}{Re}\left(\tfrac{d\bar{\mu}}{d\bar{T}}\right)\bar{T}_y\,\partial_x + \tfrac{2}{3}\tfrac{1}{Re}\left(\tfrac{d\bar{\mu}}{d\bar{T}}\right)\bar{T}_x\,\partial_y + \bar{\rho}\,\bar{u}_y \\
\mathcal{L}_{x\hat{w}} &= -\tfrac{\mathrm{i}}{3}\tfrac{\beta}{Re}\,\bar{\mu}\,\partial_x + \tfrac{2\,\mathrm{i}}{3}\tfrac{\beta}{Re}\left(\tfrac{d\bar{\mu}}{d\bar{T}}\right)\bar{T}_x \\
\mathcal{L}_{x\hat{\theta}} &= -\tfrac{1}{Re}\left(\tfrac{d\bar{\mu}}{d\bar{T}}\right)\left(\tfrac{4}{3}\,\bar{u}_x - \tfrac{2}{3}\,\bar{v}_y\right)\partial_x - \tfrac{1}{Re}\left(\tfrac{d\bar{\mu}}{d\bar{T}}\right)\left(\bar{u}_y + \bar{v}_x\right)\partial_y \\
&\quad -\tfrac{1}{Re}\left(\tfrac{d\bar{\mu}}{d\bar{T}}\right)\left(\mathrm{i}\,\beta\,\bar{w}_x + \tfrac{4}{3}\,\bar{u}_{xx} + \bar{u}_{yy} + \tfrac{1}{3}\bar{v}_{xy}\right) - \tfrac{1}{Re}\left(\tfrac{d^2\bar{\mu}}{d\bar{T}^2}\right)\left(\tfrac{4}{3}\,\bar{T}_x\bar{u}_x + \bar{T}_y\bar{u}_y + \bar{T}_y\bar{v}_x - \tfrac{2}{3}\,\bar{T}_x\,\bar{v}_y\right) \\
&\quad -\tfrac{\bar{\rho}}{\bar{T}}\left(\bar{u}\,\bar{u}_x + \bar{v}\,\bar{u}_y\right) \\
\mathcal{L}_{x\hat{p}} &= \tfrac{1}{\gamma\,M^2}\,\partial_x + \tfrac{1}{\bar{T}}\left(\bar{u}\,\bar{u}_x + \bar{v}\,\bar{u}_y\right) \\
\mathcal{R}_{x\hat{u}} &= \mathrm{i}\,\bar{\rho}
\end{aligned}
$$

Disturbance y-momentum:

$$
\begin{aligned}
\mathcal{L}_{y\hat{u}} &= -\tfrac{1}{3}\tfrac{\bar{\mu}}{Re}\,\partial^2_{xy} + \tfrac{2}{3Re}\left(\tfrac{d\bar{\mu}}{d\bar{T}}\right)\bar{T}_y\,\partial_x - \tfrac{1}{Re}\left(\tfrac{d\bar{\mu}}{d\bar{T}}\right)\bar{T}_x\,\partial_y + \bar{\rho}\,\bar{v}_x \\
\mathcal{L}_{y\hat{v}} &= -\tfrac{\bar{\mu}}{Re}\,\partial^2_{xx} + \Big[-\tfrac{1}{Re}\left(\tfrac{d\bar{\mu}}{d\bar{T}}\right)\bar{T}_x + \bar{\rho}\,\bar{u}\Big]\,\partial_x - \tfrac{4}{3}\tfrac{\bar{\mu}}{Re}\,\partial^2_{yy} + \Big[-\tfrac{4}{3Re}\left(\tfrac{d\bar{\mu}}{d\bar{T}}\right)\bar{T}_y + \bar{\rho}\,\bar{v}\Big]\,\partial_y \\
&\quad + \tfrac{\beta^2\bar{\mu}}{Re} + \bar{\rho}\,\bar{u}_x + 2\,\bar{\rho}\,\bar{v}_y + \mathrm{i}\,\beta\,\bar{\rho}\,\bar{w} + \bar{u}\,\bar{\rho}_x + \bar{v}\,\bar{\rho}_y \\
\mathcal{L}_{y\hat{w}} &= -\tfrac{\mathrm{i}}{3}\tfrac{\beta}{}\,\tfrac{\bar{\mu}}{Re}\,\partial_y + \tfrac{2\mathrm{i}}{3}\tfrac{\beta}{}\,\tfrac{1}{Re}\left(\tfrac{d\bar{\mu}}{d\bar{T}}\right)\bar{T}_y \\
\mathcal{L}_{y\hat{\theta}} &= -\tfrac{1}{Re}\left(\tfrac{d\bar{\mu}}{d\bar{T}}\right)\left(\bar{u}_y + \bar{v}_x\right)\partial_x - \tfrac{1}{Re}\left(\tfrac{d\bar{\mu}}{d\bar{T}}\right)\left(\tfrac{4}{3}\,\bar{v}_y - \tfrac{2}{3}\,\bar{u}_x\right)\partial_y \\
&\quad -\tfrac{1}{Re}\left(\tfrac{d\bar{\mu}}{d\bar{T}}\right)\left(\mathrm{i}\,\beta\,\bar{w}_y + \tfrac{4}{3}\,\bar{v}_{yy} + \tfrac{1}{3}\,\bar{u}_{xy} + \bar{v}_{xx}\right) - \tfrac{1}{Re}\left(\tfrac{d^2\bar{\mu}}{d\bar{T}^2}\right)\left(\bar{T}_x\,\bar{u}_y + \tfrac{4}{3}\,\bar{T}_y\,\bar{v}_y - \tfrac{2}{3}\,\bar{T}_y\,\bar{u}_x + \bar{T}_x\,\bar{v}_x\right) \\
&\quad -\tfrac{\bar{\rho}}{\bar{T}}\left(\bar{u}\,\bar{v}_x + \bar{v}\,\bar{v}_y\right)\Big] \\
\mathcal{L}_{y\hat{p}} &= \tfrac{1}{\gamma\,M^2}\,\partial_y + \tfrac{1}{\bar{T}}\left(\bar{u}\,\bar{v}_x + \bar{v}\,\bar{v}_y\right) \\
\mathcal{R}_{y\hat{v}} &= \mathrm{i}\,\bar{\rho}
\end{aligned}
$$

Disturbance z-momentum:

$$
\begin{aligned}
\mathcal{L}_{z\hat{u}} &= -\tfrac{\mathrm{i}}{3}\tfrac{\beta}{Re}\bar{\mu}\,\partial_x - \tfrac{\mathrm{i}}{Re}\tfrac{\beta}{}\left(\tfrac{d\bar{\mu}}{d\bar{T}}\right)\bar{T}_x + \bar{\rho}\,\bar{w}_x \\
\mathcal{L}_{z\hat{v}} &= -\tfrac{\mathrm{i}}{3}\tfrac{\beta}{Re}\bar{\mu}\,\partial_y - \tfrac{\mathrm{i}}{Re}\tfrac{\beta}{}\left(\tfrac{d\bar{\mu}}{d\bar{T}}\right)\bar{T}_y + \bar{\rho}\,\bar{w}_y \\
\mathcal{L}_{z\hat{w}} &= -\tfrac{1}{Re}\,\bar{\mu}\,\partial^2_{xx} - \tfrac{1}{Re}\,\bar{\mu}\,\partial^2_{yy} + \Big[-\tfrac{1}{Re}\left(\tfrac{d\bar{\mu}}{d\bar{T}}\right)\bar{T}_x + \bar{\rho}\,\bar{u}\Big]\,\partial_x + \Big[-\tfrac{1}{Re}\left(\tfrac{d\bar{\mu}}{d\bar{T}}\right)\bar{T}_y + \bar{\rho}\,\bar{v}\Big]\,\partial_y \\
&\quad + \tfrac{4}{3Re}\,\bar{\mu}\,\beta^2 + \bar{\rho}\,\bar{u}_x + \bar{\rho}\,\bar{v}_y + \mathrm{i}\,\beta\,\bar{\rho}\,\bar{w} + \bar{u}\,\bar{\rho}_x + \bar{v}\,\bar{\rho}_y \\
\mathcal{L}_{z\hat{\theta}} &= -\tfrac{1}{Re}\left(\tfrac{d\bar{\mu}}{d\bar{T}}\right)\bar{w}_x\,\partial_x - \tfrac{1}{Re}\left(\tfrac{d\bar{\mu}}{d\bar{T}}\right)\bar{w}_y\,\partial_y \\
&\quad -\tfrac{1}{Re}\left(\tfrac{d\bar{\mu}}{d\bar{T}}\right)\Big[\bar{w}_{xx} + \bar{w}_{yy} - \tfrac{2}{3}\,\mathrm{i}\,\beta\left(\bar{u}_x + \bar{v}_y\right)\Big] - \tfrac{1}{Re}\left(\tfrac{d^2\bar{\mu}}{d\bar{T}^2}\right)\Big[\bar{T}_x\,\bar{w}_x + \bar{T}_y\,\bar{w}_y\Big] - \tfrac{\bar{\rho}}{\bar{T}}\left(\bar{u}\,\bar{w}_x + \bar{v}\,\bar{w}_y\right) \\
\mathcal{L}_{z\hat{p}} &= \tfrac{\mathrm{i}}{\gamma}\tfrac{\beta}{M^2} + \tfrac{1}{\bar{T}}\left(\bar{u}\,\bar{w}_x + \bar{v}\,\bar{w}_y\right) \\
\mathcal{R}_{z\hat{w}} &= \mathrm{i}\,\bar{\rho}
\end{aligned}
$$

Disturbance Energy:

$$
\begin{aligned}
\mathcal{L}_{e\hat{u}} &= \left[-2\,\tfrac{\gamma\,(\gamma-1)\,M^2}{Re}\,\bar{\mu}\left(\tfrac{4}{3}\,\bar{u}_x-\tfrac{2}{3}\,\bar{v}_y\right)+\gamma\,\bar{\rho}\,\bar{T}\right]\,\partial_x-2\,\tfrac{\gamma\,(\gamma-1)\,M^2}{Re}\,\bar{\mu}\left(\bar{u}_y+\bar{v}_x\right)\,\partial_y \\
&\quad -2\,\tfrac{\mathrm{i}\;\beta\,\gamma\,(\gamma-1)\,M^2}{Re}\,\bar{\mu}\,\bar{w}_x+\bar{T}\,\bar{\rho}_x+\bar{\rho}\,\bar{T}_x \\
\mathcal{L}_{e\hat{v}} &= -2\,\tfrac{\gamma\,(\gamma-1)\,M^2}{Re}\,\bar{\mu}\left(\bar{u}_y+\bar{v}_x\right)\,\partial_x+\left[-2\,\tfrac{\gamma\,(\gamma-1)\,M^2}{Re}\,\bar{\mu}\left(-\tfrac{2}{3}\,\bar{u}_x+\tfrac{4}{3}\,\bar{v}_y\right)+\gamma\,\bar{\rho}\,\bar{T}\right]\,\partial_y \\
&\quad -2\,\tfrac{\mathrm{i}\;\beta\,\gamma\,(\gamma-1)\,M^2}{Re}\,\bar{\mu}\,\bar{w}_y+\bar{T}\,\bar{\rho}_y+\bar{\rho}\,\bar{T}_y \\
\mathcal{L}_{e\hat{w}} &= -2\,\tfrac{\gamma\,(\gamma-1)\,M^2}{Re}\,\bar{\mu}\,\bar{w}_x\,\partial_x-2\,\tfrac{\gamma\,(\gamma-1)\,M^2}{Re}\,\bar{\mu}\,\bar{w}_y\,\partial_y \\
&\quad +\tfrac{4}{3}\,\tfrac{\mathrm{i}\;\beta\,\gamma\,(\gamma-1)\,M^2}{Re}\,\bar{\mu}\left(\bar{u}_x+\bar{v}_y\right)+\mathrm{i}\;\beta\,\gamma\,\bar{\rho}\,\bar{T} \\
\mathcal{L}_{e\hat{\theta}} &= -\tfrac{\gamma\,\bar{\kappa}}{Re\;Pr}\,\partial^2_{xx}-2\,\tfrac{\gamma}{Re\;Pr}\left(\tfrac{d\bar{\kappa}}{d\bar{T}}\right)\,\bar{T}_x\,\partial_x-\tfrac{\gamma\,\bar{\kappa}}{Re\;Pr}\,\partial^2_{yy}-2\,\tfrac{\gamma}{Re\;Pr}\left(\tfrac{d\bar{\kappa}}{d\bar{T}}\right)\,\bar{T}_y\,\partial_y \\
&\quad +\tfrac{\beta^2\,\gamma\,\bar{\kappa}}{Re\;Pr}-\tfrac{\gamma}{Re\;Pr}\left(\tfrac{d\bar{\kappa}}{d\bar{T}}\right)\left(\bar{T}_{xx}+\bar{T}_{yy}\right)-\tfrac{\gamma}{Re\;Pr}\left(\tfrac{d^2\bar{\kappa}}{d\bar{T}^2}\right)\left(\bar{T}^2_x+\bar{T}^2_y\right) \\
&\quad -\tfrac{\gamma\,(\gamma-1)\,M^2}{Re}\left(\tfrac{d\bar{\mu}}{d\bar{T}}\right)\left(\tfrac{4}{3}\,\bar{u}^2_x+\bar{v}^2_x+\bar{w}^2_x+\bar{u}^2_y+\tfrac{4}{3}\,\bar{v}^2_y+\bar{w}^2_y-\tfrac{4}{3}\,\bar{u}_x\,\bar{v}_y+2\bar{u}_y\,\bar{v}_x\right) \\
\mathcal{L}_{e\hat{p}} &= \bar{u}\,\partial_x+\bar{v}\,\partial_y+\mathrm{i}\;\beta\,\bar{w}+\gamma\left(\bar{u}_x+\bar{v}_y\right)
\end{aligned}
$$

$$
\mathcal{R}_{e\hat{p}} = \mathrm{i}
$$

Disturbance Continuity:

$$
\begin{aligned}
\mathcal{L}_{c\hat{u}} &= \bar{\rho}\,\bar{T}\,\partial_x+\bar{T}\,\bar{\rho}_x \\
\mathcal{L}_{c\hat{v}} &= \bar{\rho}\,\bar{T}\,\partial_y+\bar{T}\,\bar{\rho}_y \\
\mathcal{L}_{c\hat{w}} &= \mathrm{i}\;\beta\,\bar{\rho}\,\bar{T}\,\hat{w} \\
\mathcal{L}_{c\hat{\theta}} &= -\bar{\rho}\,\bar{u}\,\partial_x-\bar{\rho}\,\bar{v}\,\partial_y-\bar{\rho}\,\bar{u}_x-\bar{\rho}\,\bar{v}_y-\mathrm{i}\;\beta\,\bar{\rho}\,\bar{w}-\bar{u}\,\bar{\rho}_x-\bar{v}\,\bar{\rho}_y+\tfrac{\bar{\rho}}{\bar{T}}\left(\bar{u}\,\bar{T}_x+\bar{v}\,\bar{T}_y\right) \\
\mathcal{L}^G_{c\hat{p}} &= \bar{u}\,\partial_x+\bar{v}\,\partial_y+\mathrm{i}\;\beta\,\bar{w}+\bar{u}_x+\bar{v}_y-\tfrac{1}{\bar{T}}\left(\bar{u}\,\bar{T}_x+\bar{v}\,\bar{T}_y\right)
\end{aligned}
$$

$$
\begin{aligned}
\mathcal{R}_{c\hat{\theta}} &= -\mathrm{i}\;\bar{\rho} \\
\mathcal{R}_{c\hat{p}} &= \mathrm{i}
\end{aligned}
$$